


Compact hybrid electrohydraulic actuators using smart materials: A review

Journal of Intelligent Material Systems and Structures
23(6) 597–634
© The Author(s) 2011
Reprints and permissions:
sagepub.co.uk/journalsPermissions.nav
DOI: 10.1177/1045389X11418862
jim.sagepub.com


Anirban Chaudhuri and Norman Wereley

Abstract

The development of compact hybrid electrohydraulic actuators driven by various smart materials has been widely reported in the literature in recent years. Such solid-state-induced strain actuators have applications in a variety of aerospace and automotive and mechanical engineering fields. These devices are capable of producing high stroke (or displacement) and high force (or pressures) in a compact form factor by utilizing the large bandwidth and energy density of currently available smart materials. The basic operation of these hybrid actuators involves high-frequency bidirectional operation of an active material that is converted to unidirectional motion of a hydraulic fluid by a set of valves. Over the last decade, several prototype hybrid actuators have been designed using piezoelectric (PZT-5H), magnetostrictive (Terfenol-D), and electrostrictive (PMN-PT) materials as the driving elements, with actuation frequencies ranging from 10 Hz to 1 kHz. Power outputs and volumetric flow rates have reached up to 20 W and 40 cm³/s, respectively. Different mathematical models have been developed to evaluate the performance of these hybrid actuators. While early efforts focused on a simple, quasi-static approach to simulate pump operation, more complex dynamic models have been recently developed to capture the complex interaction between the smart material and the transmission fluid at high operating frequencies. The objective of this survey is to review the state-of-the-art in compact hybrid electrohydraulic actuation systems and to summarize design and modeling efforts.

Keywords

smart materials, compact hybrid actuators, electro-hydraulic actuators, frequency rectification, smart hydraulic actuator

Introduction

Present-day hydraulic actuators typically rely on a central supply of high-pressure fluid along with a controllable servovalve to distribute this fluid to hydraulic output devices, where the pressurized fluid does useful mechanical work. Conventional hydraulic actuators offer high bandwidth and authority in very compact packages, but their need for hydraulic fluid lines can make them unsuitable for distributed actuation applications like those found on the unmanned combat air vehicle (UCAV). Although such actuators are effective in numerous applications, benefits would accrue from more efficient, high-bandwidth devices that can be distributed across the airframe by eliminating the central hydraulic supply. The challenges are even greater in rotorcraft as many of the important applications for noise and vibration control such as active flaps and active pitch links (APLs) must operate in the rotating frame; the actuation of an aerodynamic surface in such situations cannot be achieved through conventional hydraulic or electric methods due to the prohibitive high-g centrifugal force field

environment generated during blade rotation (Giurgiutiu et al., 1995). A compact, high-bandwidth, electrically powered actuator for use in smaller vehicles as well as in rotating environments is required.

Solid-state actuators using smart materials provide an effective way to implement this strategy (Crawley, 1987; Barsoum, 1997; Claeysen et al., 1997; Loewy, 1997; Chopra, 2000; Giurgiutiu, 2000; Anderson et al., 2003). Although output displacement of these materials is very small (approximately in micrometer), they can produce very high forces and can be operated at high frequencies (Niezrecki et al., 2001). By using inherently energetic smart materials to drive a compressed fluid directly, the complexity of transduction is reduced, while central fluid supplies and transfer lines can be

Dept. of Aerospace Engineering, University of Maryland, College Park MD 20742 USA

Corresponding author:

Norman Wereley, Professor and Associate Chair, Department of Aerospace Engineering, University of Maryland, College Park, MD, USA.
Email: wereley@umd.edu

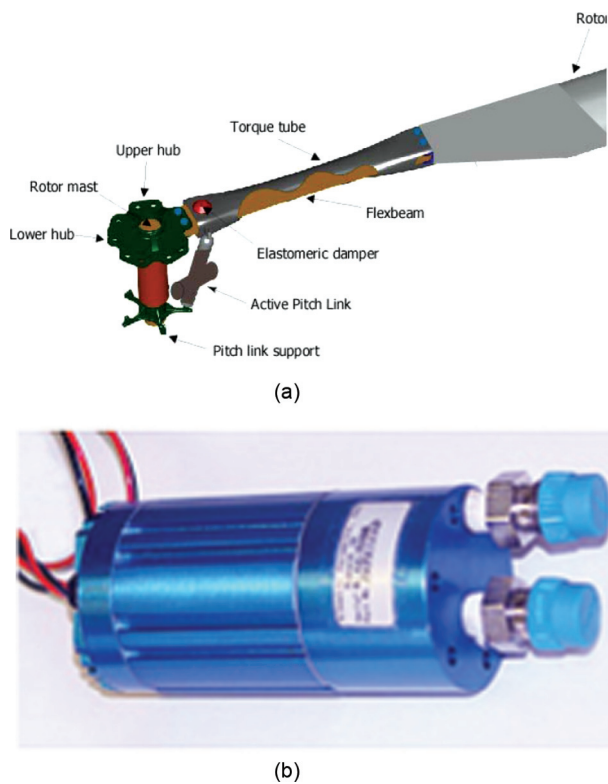


Figure 1. Applications of compact hybrid hydraulic actuators in various industries (a) APL (Sirohi, 2002) (b) Variable flow fluid pumps (Kinetic Ceramics Inc.).

eliminated by operating in a closed-fluid system. Applications targeted by this development begin with those currently employing hydraulic and ballscrew actuators as well as those that are not feasible because of limitations in present-day devices.

Over the last decade, there has been significant research activity in the development of hybrid hydraulic actuators driven by various smart materials; the Compact Hybrid Actuator Program (CHAP) at DARPA initiated much research and development in the area of developing new types of electromechanical actuators and devices that take advantage of the high energy density of smart material elements (Garcia, 2002). The evolutionary step for these transduction elements was for their incorporation into devices with high power density and/or high specific power, so that these compact hybrid actuators could potentially supplant traditional actuation systems while reducing the overall power and space consumed, thus the interest in applications requiring distributed actuator systems such as adaptive airframes and robotic locomotion. A secondary goal of this technology development was the creation of devices and systems that allow application of mechanical power output through hydraulics without the need for traditional hydraulic distribution lines (Anderson and Garg, 2002; Bouchilloux et al., 2004). An innovative application in the rotorcraft

industry could be APLs for individual blade control (Figure 1(a)); such devices would be compact while offering much higher stroke and bandwidth capabilities in comparison with hydraulically powered mechanical pitch links currently in use (John et al., 2009). In the automotive industry, similar actuation systems with simpler structure and compact size have been explored to replace conventional electrohydraulic actuators for automatic transmissions. There have also been some investigations for application in biomedical fields involving low flow rates (Cheng et al., 2007).

The use of a hydraulic fluid and valve system for frequency rectification is an effective way to overcome the problem of small displacements from currently available smart materials and to develop a moderately high-force, large-stroke smart actuator ideal for such applications. The basic operation of these hybrid actuators involves high-frequency bidirectional operation of the active material, piezoelectric, magnetostrictive, or electrostrictive, which is converted to unidirectional motion of the transmission fluid by a set of valves by flow rectification in each cycle using a set of valves. Through this stepwise actuation process, the high-frequency, small stroke of the active material is converted into a lower frequency, larger displacement of the output cylinder.

At high driving frequencies, the inertial effects of the fluid mass dominate over the viscous effects and the problem becomes unsteady in nature. Geometrical parameters of the flow path and compressibility of the fluid transmission medium are also important. Mathematical models of the hydraulic hybrid actuator have been developed to show basic operational principle under different operating conditions and to capture the phenomena affecting system performance. Initial modeling efforts used a simple, quasi-static approach to match mechanical impedances of the driving smart material with the driven fluid medium and derive maximum electromechanical conversion efficiencies; more complex models developed over the last few years also include the frequency-dependent electromechanical transduction behavior, unsteady flow in the manifold, and losses in the valves. Computational fluid dynamics (CFD) has also been applied in some cases to quantify the flow behavior.

Operation of a Smart Electrohydraulic Pump

The starting point of a smart material-driven hydraulic actuator is the initiation of flow because of the oscillation of a mechanical piston being driven by the extension/contraction of a smart material upon application of a sinusoidal electrical input. For electroactive materials like piezoelectrics (e.g., lead zirconate titanate (PZT-5H)) and electrostrictives (e.g., lead magnesium

niobate-lead titanate (PMN-PT)), an electric field is applied to the active stack; in the case of magnetostrictive materials like Terfenol-D, actuation is obtained by using a magnetizing coil placed around a cylindrical rodlike element. The choice of active material depends upon several factors, of which free induced strain, elastic modulus, high-frequency operation, drive voltage levels, and cost are most important; a comparison between different smart materials for such applications was done by Giurgiutiu and co-workers (Giurgiutiu and Rogers, 1996; Giurgiutiu et al., 1996).

Electroactive Materials

Piezoelectrics are widely considered for smart actuator designs because they are lightweight and compact, relatively inexpensive, and exhibit moderately linear field-strain relations at low drive levels. They also exhibit broadband drive capabilities, an important property when designing compact smart pumps with high flow rates. However, the piezoelectric materials exhibit hysteresis and constitutive nonlinearities at all drive levels (Mitrovic et al., 1999). For high drive regimes, it might be necessary to either employ charge or current control or use models and control designs, which incorporate the hysteresis to achieve high accuracy tracking. In certain applications, electrostrictive transducers constructed from relaxor ferroelectric materials are advantageous over piezoelectric materials because they exhibit minimal hysteresis and are not poled and hence exhibit few aging effects. However, their highly temperature-dependent and nonlinear saturation behavior must be accommodated when designing complex systems that incorporate these compounds. Due to the use of structural adhesives to glue the electroactive layers and to assemble electrodes, the final stack stiffness is significantly lower than the basic ceramic material with same geometry. Care must be taken to ensure that the active element is aligned correctly and subjected to a compressive load under all conditions as these materials have very low tensile strength. The electrical power supply should also be chosen to deliver the required reactive input power, and proper insulation should be used at the high voltages.

Magnetoactive Materials

The magnetic analogues of electrostrictive compounds are magnetostrictive materials that convert magnetic energy into mechanical energy and vice versa. Due to the circuits required to generate the required magnetic fields, transducers that use magnetostrictive cores are currently larger and more massive than piezoelectric or electrostrictive stacks. However, the giant forces and moderate strains generated by the transducers make them advantageous in certain applications. At moderate to high drive levels, the nonlinearities and

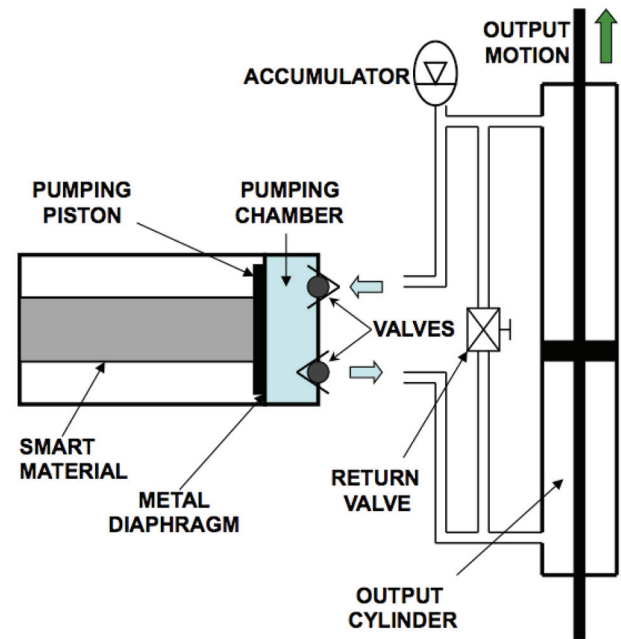


Figure 2. Schematic of unidirectional smart hybrid actuator operation.

bandwidth limitations must be accommodated before magnetostrictives can be used to their full potential. As the magnetostrictive actuator is a current-driven device, lower voltages are required; this makes it simpler to develop the power supply.

A typical hybrid pump uses the principle of frequency rectification to produce a net flow rate out of the pump; this is performed by unidirectional valves housed within the pumping head (Figure 2), which allow fluid flow either out of the pumping chamber (through the discharge port) or into the pumping chamber (through the intake port).

The hybrid pumping device operates in four distinct stages as follows (Nasser et al., 2000; John et al., 2008; Chaudhuri et al., 2009):

1. *Compression:* The first stage involves the expansion of the hybrid material stack/rod as an increasing magnetic field is applied. This in turn compresses the fluid in the pumping chamber, resulting in an increase in chamber pressure. This stage continues as long as the pressure difference across the valve is less than the valve cracking pressure. The intake valve is closed during this stage as the pressure in the chamber is greater than the pressure in the intake tube of the pump.
2. *Discharge:* In the second stage, the pressure difference between the chamber and the discharge tube becomes large enough to open the discharge valve and fluid starts to flow out of the chamber into the discharge tube. Pressure builds

up in the high-pressure side of the output cylinder and results in motion of the output shaft, causing fluid to move from the low-pressure-driven side of the output cylinder into the highly compliant accumulator that is maintained at almost constant pressure.

3. *Expansion:* In this stage, the current in the coil starts decreasing causing the hybrid stack to retreat and the pumping chamber pressure reduces. The intake reed valve is designed to only allow flow of fluid into the pumping chamber, whereas the discharge reed valve port does not allow any fluid to come into the chamber. However, the intake port is still closed as the difference between the accumulator and pumping chamber pressures is still lower than the cracking pressure. This stage is similar to the compression stage, except that the stack/rod is contracting instead of expanding as in Stage 1.
4. *Intake:* In the final *intake* stage, the pumping chamber pressure drops further and the pressure difference between the chamber and the intake tube becomes large enough to crack open the intake reed valve and allow fluid flow back into the chamber.

These four stages, depicted in Figure 3, are repeated every pumping cycle and result in a net mass flow rate out of the pump through the discharge tube and an equivalent mass flow rate into the pump through the intake tube.

To transfer the pressure generated within the pumping chamber to an external device or application, a

manifold is used to connect the hybrid pump to an output cylinder; this manifold also houses the accumulator port and the return valve (for unidirectional operation). The return valve is closed during normal operation and is only used to reset the output piston to its original position at the end of each stroke. The accumulator consists of a nitrogen gas chamber with a rubber diaphragm; the pressure in the chamber decides the bias pressure being applied to the fluid. Fluid from the output port of the hybrid pump flows through the manifold and into the output cylinder, causing an increase in pressure. As the other end of the output cylinder is connected to the highly compliant accumulator that is maintained at the bias pressure, the output piston shaft moves due to the pressure difference between the two chambers of the cylinder.

Although theoretically attractive, practical limitations arise that limit the efficacy of the solid–fluid hybrid actuation approach. In particular, inertial loads, fluid viscosity, and compressibility combine with loss mechanisms inherent in the active material to limit the effective bandwidth of the driving actuator and the total actuator output power (Giurgiutiu et al., 1996; Nasser and Leo, 2000). Care must be taken in the design of the system to match the mechanical impedance characteristics of the driving element to the fluid transmission, so that maximum efficiency of operation is obtained (Leo, 2007; Kan et al., 2009).

Recent Developments

Some of the compact hybrid actuators developed in recent times are as follows:

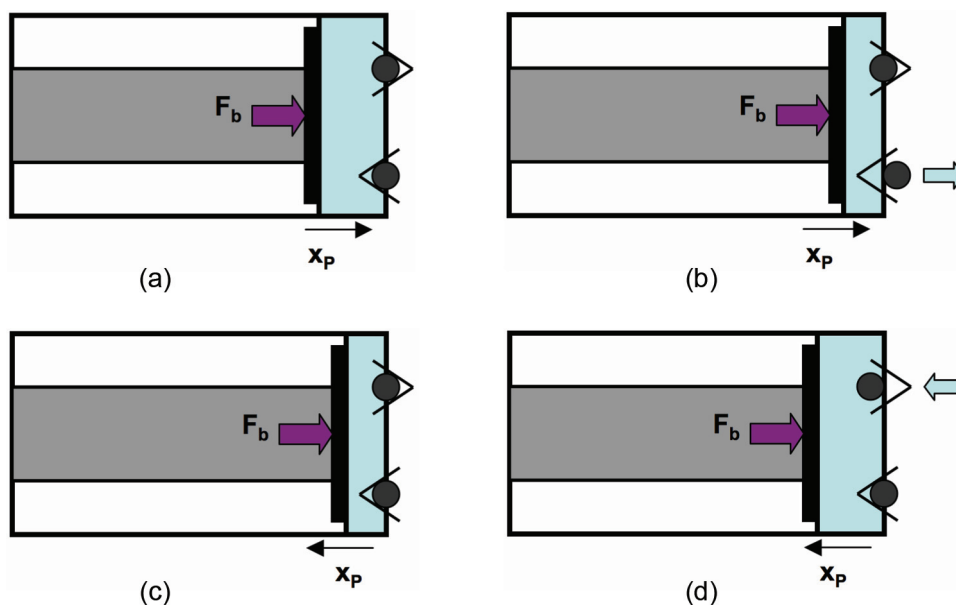


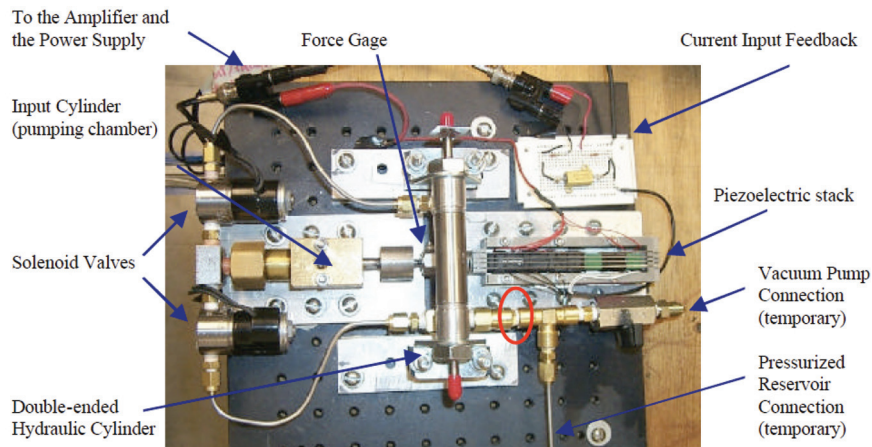
Figure 3. Operating stages of a hybrid pump in every cycle: (a) compression, (b) discharge, (c) expansion, and (d) intake.

1. One of the first-reported hybrid hydraulic actuators was the piezoelectric stack-based actuator developed by Konishi and co-workers (Konishi et al., 1993; Konishi, 1995), which had a maximum power output of 34 W and a peak pumping frequency of around 300 Hz and a static bias pressure of 3.0 MPa. The device was constructed using a multilayer piezoelectric element 22 mm in diameter and 55.5 mm in length. The hydraulic circuit was filled with a working liquid, and a static pressure was applied to (1) prevent cavitation in the pump, (2) apply a preset load to the piezoelectric element, and (3) to push the piston rod out of the cylinder. The control valve was operated by the pilot pressure generated by the pump. A simple model based on a single-degree-of-freedom (SDOF) model of the output actuator was used to design an observer and to control the output motion.
2. Tang et al. (1995) developed a piezohydraulic actuator for active vibration control of rotor-dynamic systems. The actuator was built to transfer the high-force, high-frequency capability of the piezoelectric driver to a hydraulic system; the piezoelectric pusher forced the input piston which in turn forced the column of hydraulic fluid into the output piston. Polyvinyl chloride (PVC)-based liquid plastics (LP) were used in this setup because they have a thick texture that prevents leakage and a high bulk modulus for transmitting even the smallest motions associated with vibration control. From test results, the designers concluded that the output stroke depended on the ratio of the piston areas, compressibility of the LP, tube flexibility, and impedance encountered by the output piston.
3. A magnetostrictive stack-based water pump was developed by Gerver et al. (1998); this device employed hydraulic stroke amplification techniques and produced power output of less than 1 W. This design used Terfenol-D as the driving element and employed stroke amplification to obtain high flow rates. The pump achieved a flow rate of 15 mL/s at 5 psi with a power input of 41 W. According to the designers, higher flow rates were obtained by either lowering the pressure (32.5 mL/s at 1.2 psi) or raising the input power (22 mL/s at 5 psi consuming 141 W). To avoid valve inertia at high operating frequencies, thin rigid disks of stainless steel were used. The maximum operational frequency was 150 Hz.
4. Mauck and co-workers (Mauck and Lynch, 1999, 2000; Mauck et al., 2000) developed a piezoelectric stack-based device that produced around 4 W and had a blocked force of 271.7 N (61 lbf); however, it operated at relatively low pumping frequencies (less than 100 Hz) and performed frequency rectification using passive valves. The stack actuator selected was a soft PZT, which maximized output displacement at the cost of a large loss tangent (high hysteresis). This resulted in the generation of significant heat when the operating frequency was increased and verified the belief that without the introduction of a cooling system, continuous operation of the stack above 60 Hz would lead to stack self-heating to the point of failure.
5. Nasser et al. (2000) developed a piezo-based actuator that was capable of 4.5 W output power and operated at slightly higher pumping frequencies of around 200 Hz. The major difference between this work and previous research was the use of fluid compressibility to eliminate the need for hydraulic accumulators and four-way control valves. The piezoelectric actuator stack was rated for 100 μm of free displacement and 3000 N of blocked force for a peak-to-peak input voltage of 150 V. A cylinder displacement of 113 μm at a frequency of 10 Hz was measured under these test conditions. Friction was not deemed a limiting factor in the development of the piezohydraulic actuation system. This design was improved upon by the addition of active valves for rectification (Hurst, 2002; Tan, 2002; Tan et al., 2005). Tests were conducted to measure the hydraulic cylinder velocity under no load and with a 12.63 kg load. The timing and phase offset of the active valves were studied; for frequencies lower than 100 Hz, it was concluded that valve timing could change the output velocity by 20%–30% when the duty cycle was greater than 50% and the valve offset was positive.
6. A compact hybrid hydraulic actuation device for an APL usable in swashplateless helicopter rotors was developed by Sirohi and Chopra (Sirohi, 2002; Sirohi and Chopra, 2001, 2003; Ellison, 2004; Ellison et al., 2004) at the University of Maryland. Using piezoelectric stacks, this actuator had an output power of 2.5 W, blocked force of around 138 N (31 lbf) and operated at relatively higher pumping frequencies. The maximum pumping frequency of 1 kHz was decided on the basis of temperature limits of the piezostacks. As precise measurement of the blocked force of the device was difficult, the value of blocked force was obtained by fitting a straight line to the force–velocity data and extrapolating it to the zero velocity

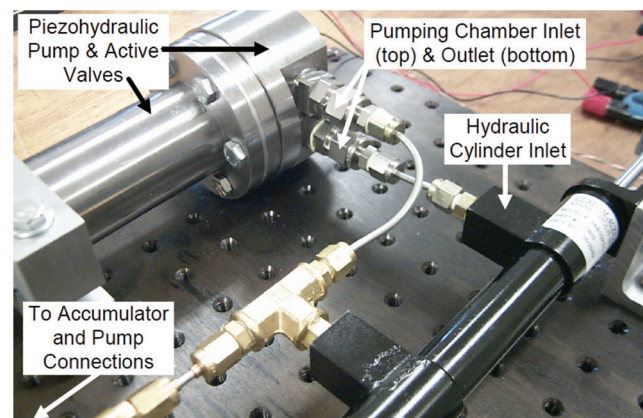
condition. Two 2-way spool valves were added to the hydraulic circuit for bidirectional operation. At higher pumping frequencies, significant losses in flow rate were observed, and testing of this device revealed a highly non-linear variation of the output velocity with pumping frequency. A comparison of actuator performance with other smart materials (Figure 8) in a modified pump body was carried out by John et al. (2006, 2007). In each case, the active material had a length of around 54 mm and cross-sectional area of 25 mm². While the maximum power output of 2.5 W was obtained for the Terfenol-D and PMN-based devices, the latter produced the highest no-load output velocity of 270 mm/s and electromechanical efficiency of 7%. The effect of centrifugal loads on the performance of the prototype device was investigated by testing under rotation in the vacuum whirl test chamber (John et al., 2009); the centrifugal loading on the actuator was nominally higher than the

full-scale centrifugal load experienced by a UH-60 pitch link (Figure 4). It was shown that the addition of thrust bearings to the spool valve shaft enabled successful operation in high-g centrifugal force fields.

- Lee et al. (2004) developed a piezoelectric-hydraulic pump using active unimorph disk valves for frequency rectification; they reported output flow rate of 3.4 cm³/s, specific energy density of 12 W/kg, and a stall pressure of 8.3 MPa (1204 psi). According to the authors, the unimorph disk valve concept includes a large flow area with low lift and an unidirectional flow from inlet to pumping chamber and to outlet. Application of a voltage to the unimorph disk valves causes the valves (metal disk layer) to deflect away from the seat, opening more rapidly than a conventional check valve and reducing flow resistance. Back flow that normally accompanies passive valve operation could also be suppressed. The outlet valve opened before the piezoelectric stack actuator



(a)



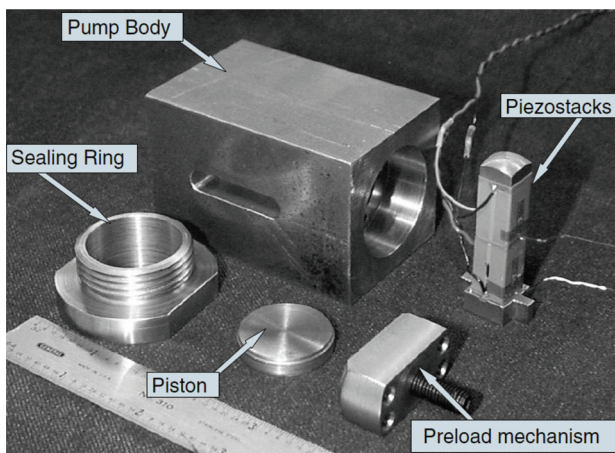
(b)

Figure 4. Piezohydraulic devices developed at Virginia Tech: (a) piezohydraulic pump developed by Nasser (2000) and (b) compact hybrid actuator with piezopump and hydraulic cylinder developed by Hurst (2002).

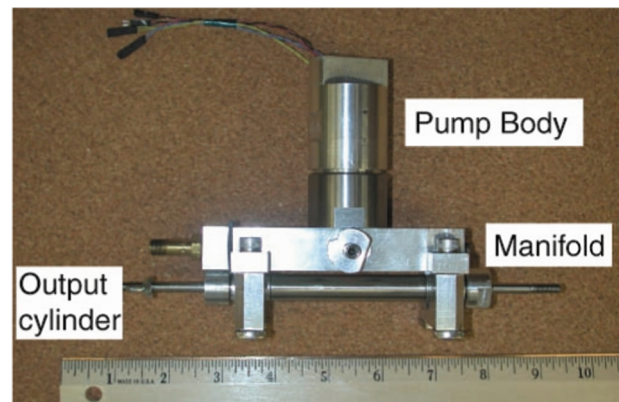
- started its stroke within an optimized duty cycle, so that the delivered fluid volume could be maximized. A later version of this piezohydraulic actuator produced a power output of 46 W by using proprietary microelectromechanical systems (MEMS)-based valves from Kinetic Ceramics, Inc., along with a commercially available piezopump (Tieck et al., 2005). The MEMS array valve was 1.18 cm in diameter and 0.033 cm thick and held approximately 84 individual valves. The output flow rates were $8.5 \text{ cm}^3/\text{s}$ and $17 \text{ cm}^3/\text{s}$ at actuation frequencies of 500 Hz and 1 kHz, respectively. However, when commercially available check valves were attached to the pump, the maximum flow rate was $0.9 \text{ cm}^3/\text{s}$ and the output power was 0.2 W. According to the authors, the reason for this significant drop was the increase of system compliance caused by moving the valves external to the pump housing and air entrapment.
8. Ullmann (Ullmann et al., 2001; Ullmann and Fono, 2002) developed a valveless hybrid pump that used appropriately shaped and directed nozzles to rectify the flow initiated by oscillatory motion of a diaphragm, similar to the conventional piston reciprocating pumps; the pumping action was produced by activating a piezoelectric disk that was glued to a stainless steel (or any other metal) disk. The driving voltage on the piezoelectric device was converted into force acting on the center of the disk, resulting in a deflection. This device was of much smaller scale than the actuators mentioned earlier and had a flow rate of $0.2 \text{ cm}^3/\text{s}$ with pressure of around 90 kPa (13 psi). This pump, however, did not have a flow

rectification system and worked by transferring fluid from a high-pressure source to a low-pressure sink at certain frequencies. Ullmann and Fono (2002) reported that the best performance (maximum flow rate and pressure drop) was obtained at the natural frequency, which was sensitive to fluid masses and geometry in the inlet/output lines, and was much lower than the natural frequency of the disk/piezoelectric device assembly without the liquid (Figure 5).

9. Chapman et al. (2005) developed three small, low-cost piezohydraulic pumps to deliver up to 600 psi (4.1 MPa) of blocked pressure and $5.63 \text{ cm}^3/\text{s}$ of free flow; the smallest pump weighed less than 90 g. A four-way spool valve was used for bidirectional control of the output linear actuator. The first set of experiments using check valves produced flow rates up to $1.2 \text{ cm}^3/\text{s}$ between 100 and 120 Hz pumping frequencies; it was noted that an increase in bias pressure actually affects pump performance and was attributed to the increased friction in the hydraulic actuator seals. A second design incorporating reed valves yielded the best performance at 400 Hz pumping frequency. Though the reed valves (0.010 and 0.005 in thick) were designed for a natural frequency of 2 kHz in air, it was noticed that their performance dropped sharply for frequencies more than 400 Hz and never recovered.
10. A piezoelectric-hydraulic pump (PHP) was developed for use in automotive transmissions at the University of Michigan by Kim and Wang (2007, 2009). The PHP device consisted of a PZT stack transducer, which was actuated by a high-frequency input voltage, a gas



(a)



(b)

Figure 5. First-generation piezohydraulic devices developed at the University of Maryland (a) piezohydraulic pump developed by Sirohi (2002) and (b) compact hybrid actuator with piezopump and hydraulic cylinder developed by John (2007).

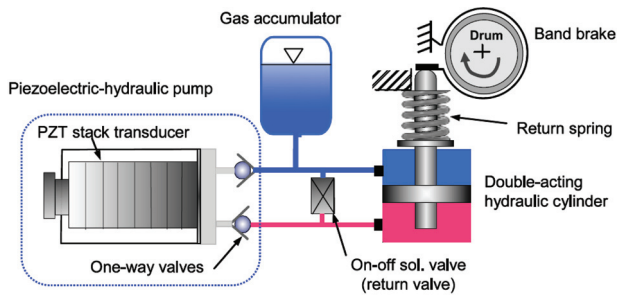


Figure 6. Piezoelectric-hydraulic pump developed at the University of Michigan by Kim and Wang (2007).

accumulator, and a double-acting hydraulic cylinder (Figure 6). To minimize the size, complexity, and weight of an active piezoelectric-based active valve system, two passive reed valves were fabricated to achieve the one-way valve functions. The accumulator provided the various essential functions, which included pumping, preventing cavitations, and determining deadhead pressure (the maximum pressure at the outlet of the actuation system with the cylinder piston locked). As bidirectional action was not required for AT shift control, a normally closed type on-off solenoid valve was incorporated for releasing the actuating pressure. The maximum flow rate was $19 \text{ cm}^3/\text{s}$ at 230 Hz pumping frequency under an accumulator pressure of 0.4 MPa, and the peak deadhead pressure developed was 0.55 MPa.

11. Hybrid actuators driven by piezoelectric (Yoo et al., 2003, 2005; Yoo and Wereley, 2004) and magnetostrictive (Nosse and Dapino, 2005; John et al., 2007) materials in conjunction with magnetorheological fluids (MRFs) for bidirectional control have also been developed in recent times. Important advantages of this valve system over mechanical valves are the lack of moving parts and faster response, whereas the major disadvantage is that full closure of the valve is never possible due to the finite yield stress and creep of the MRF. The MR valves used in the Smart Structures Laboratory at the University of Maryland, College Park, used the controllable yield stress of MRFs (Wereley and Pang, 1998; Lee and Wereley, 1999; Wereley, 2008) to effectively open or close the channels that comprise opposite arms of an H-bridge, ultimately leading to directional control of the output shaft (Yoo and Wereley, 2002; John et al., 2008). The maximum output shaft velocity obtainable from the system was around 50 mm/s at a pumping frequency of 125 Hz, which was much lower than the peak velocity and

resonant frequency noticed in a piezohydraulic actuator using hydraulic oil. In the MR-based device developed by Nosse and Dapino (2007) at the Ohio State University, flow generated by a Terfenol-D pump was routed through two flow paths connected in parallel, while solenoids were used to alternatively activate the fluid in either ends of the passages.

Commercial Developments

There have been hybrid hydraulic actuator developments among commercial establishments too. Active Signal Technologies (Bridger et al., 2004) developed a magnetostrictive water pump operating at 3000 psi (21 MPa) pressure with a no-load flow rate of $57 \text{ cm}^3/\text{s}$ ($3.5 \text{ inch}^3/\text{s}$). The Terfenol rod used initially in this test setup was 4 inch (101 mm) long \times 1.25 inch (32 mm) diameter but could not achieve the desired specifications. An inertial mass (*Tonpilz*)-based design was then used to improve the performance and increase the operational frequency to $\sim 2 \text{ kHz}$. Optimum matching for a 1 inch (25.4 mm) diameter \times 3.125 inch (79.4 mm) long Terfenol rod was achieved with a 1.25 inch (32 mm) diameter piston and 0.1 inch (2.5 mm) chamber height. Under the smart material actuated servo hydraulics (SMASH) program, CSA Engineering Inc. (Anderson and Garg, 2002; Anderson et al., 2002, 2003; Lindler et al., 2003) reported the development of several hybrid actuators, including a magnetostrictive hydraulic actuator with a power output exceeding 100 W (Sneed et al., 2006, 2007). The maximum no-load flow rate was 0.4 gpm ($25.2 \text{ cm}^3/\text{s}$), and the maximum developed pressure was 1700 psi (11.7 MPa). A 4 inch (102 mm) long, 1 inch (25.4 mm) diameter Terfenol-D rod was used for actuation, and the optimal operating frequency was 200 Hz. Reed valves were used for flow rectification; according to the authors, insufficiently stiff reeds can lead to “valve float” where the valves fail to close completely between cycles allowing back flow through the pump, whereas excessive stiffness reduces maximum reed displacement causing higher pressure drops. Kinetic Ceramics, Inc. developed piezoelectric fluid pumps with maximum flow rates up to $40 \text{ cm}^3/\text{s}$ and a stall pressure of 2500 psi (17.2 MPa). Cedrat Technologies has developed several actuators based on piezoelectric (Petitniot et al., 2002) and magnetostrictive (Claeyssen and Lhermet, 2002; Lhermet et al., 2006) materials for implementation over wide frequency ranges (Figures 7 and 8). Several patents dealing with hybrid hydraulic actuation using both electroactive and magnetoactive materials have also been published (Beckman and Blickstein, 1984, 1985; Culp and Nuys, 1993; Sager and Matice, 1998; Ogawa et al., 1999; Bishop et al., 2000; Bridger et al., 2004).

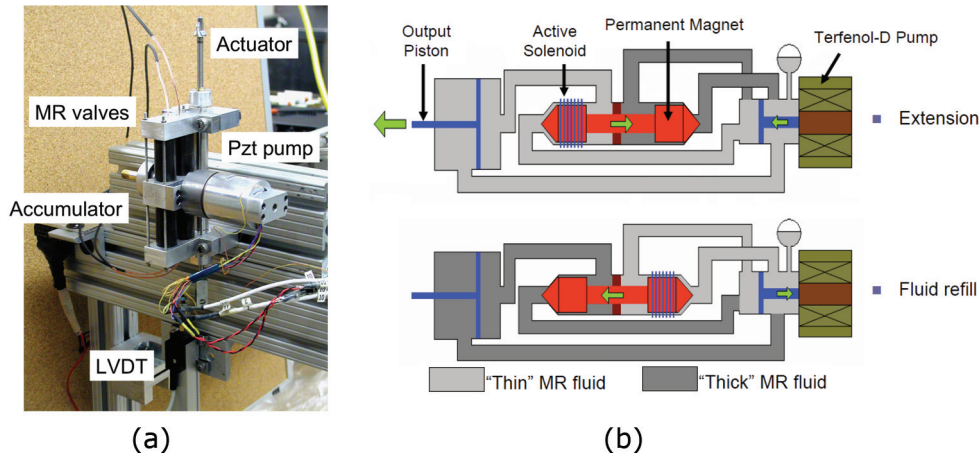


Figure 7. Bidirectional compact actuation devices using smart materials with a MRF: (a) piezo-MR pump developed at UMD by Yoo et al. (2004) and (b) Terfenol-based pump with MR-controlled valves by Nosse and Dapino (2005).

Experimental Setup and Device Performance Tests

Preliminary Design

The initial design of the pumping device is based on the specified no-load velocity, v_L , and blocked force, F_b . The fluid in the manifold tubing is assumed to be incompressible, whereas the fluid in the pumping chamber is compressible. Under idealized quasi-static conditions, the output volume flow rate, Q , can be calculated from the no-load velocity requirements (Chaudhuri and Wereley, 2010).

$$Q = A_o \times v_L, \quad (1)$$

where $A_o = \pi(d_o^2 - d_i^2)/4$ is the cross-sectional area of the output cylinder with bore d_o and shaft diameter d_i . For an incompressible fluid being pumped at frequency f by an actuator stack/rod with length L_a and strain ε , the volume flow rate is also given by

$$Q = f \times \varepsilon \times L_a \times A_{ch}, \quad (2)$$

where $A_{ch} = \pi D_{ch}^2/4$ is the area of the pumping chamber piston of diameter D_{ch} (John et al., 2006). Combining Equations (1) and (2), we can calculate active material length, L_a , for specified no-load velocity, v_L , at particular pumping frequency and induced strain as follows:

$$L_a = \left(\frac{v_L}{\varepsilon f} \right) \times \left(\frac{A_o}{A_{ch}} \right). \quad (3)$$

For small piston displacements, the pressure generated within the pumping chamber is a linear function of the fluid bulk modulus, β , as follows (Regelbrugge et al., 2003; Sirohi and Chopra, 2003; Tan et al., 2005; Chaudhuri et al., 2009):

$$P_b = \beta(x_P/L_{ch}). \quad (4)$$

This is equal to the pressure in the output cylinder, F_b/A_o , under blocked conditions (Chaudhuri and Wereley, 2010); hence,

$$x_P = (F_b/K_{ch}) \times (A_{ch}/A_o), \quad (5)$$

where

$$K_{ch} = \beta A_{ch}/L_{ch} \quad (6)$$

is the stiffness of the fluid pumping chamber (Sirohi and Chopra, 2003). Using this along with the stiffnesses of the actuator stack, K_a , the actual strain induced in the active material is obtained from the static free induced displacement, x_{free} , as follows (Giurgutiu et al., 1997; Sirohi and Chopra, 2003):

$$x_P = \frac{K_a}{K_a + K_{ch}} x_{free} \Rightarrow K_a = \frac{K_{ch}}{\frac{x_{free}}{x_P} - 1}. \quad (7)$$

By definition, $K_a = E_a A_a/L_a$ for an actuator with cross-sectional area $A_a = \pi D_a^2/4$, where D_a is the diameter of the active rod/stack. Using Equation (7) along with the value of L_a , D_a can be calculated.

Hybrid Pump Construction

Hybrid electrohydraulic actuators, using the giant magnetostrictive material Terfenol-D ($Tb_{0.3}Dy_{0.7}Fe_{1.92}$) and the single-crystal electrostrictive material PMN-PT (chemical composition: $(1-x)Pb(Mg_{1/3}Nb_{2/3})O_{3-x}PbTiO_3$) as the respective driving elements, were developed at the University of Maryland (Chaudhuri, 2008; Chaudhuri et al., 2009; Chaudhuri and Wereley, 2010). Hydraulic oil was used as the fluid medium for transmission of energy. Rectification of the oscillatory fluid motion was achieved using passive reed valves made of spring steel. The performance of the actuator, in terms of maximum flow rate and blocked force, was measured by varying the

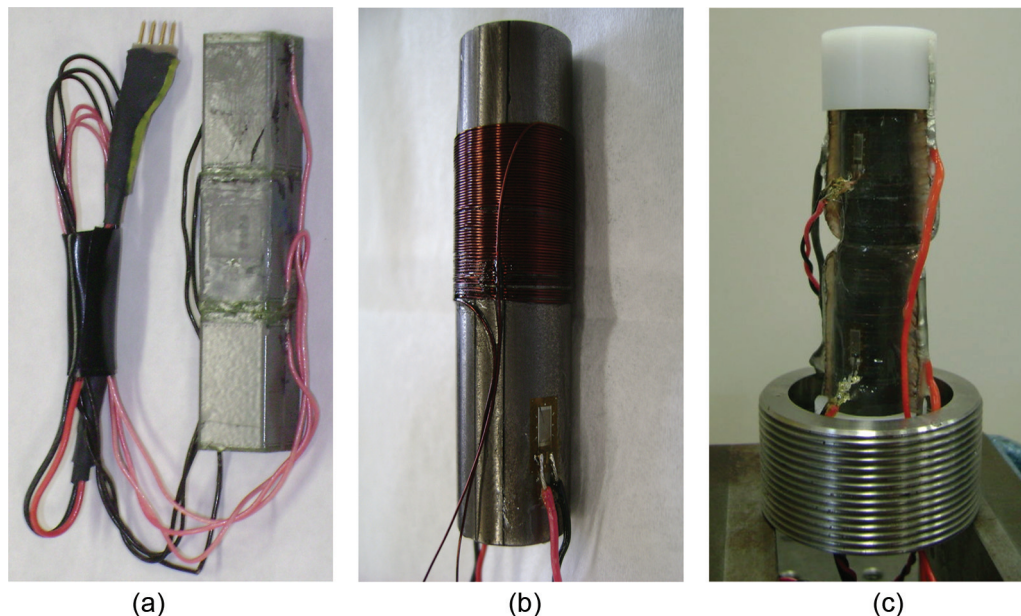


Figure 8. Different smart materials used in hybrid electrohydraulic actuators: (a) PZT-5H actuator stack with electrical connectors, (b) laminated Terfenol-D rod with strain gage and magnetic flux sense coil, and (c) stacked PMN actuators with strain gages and insulating caps.

pumping frequency, input electrical current (or voltage), and the fluid bias pressures. The displacement of the output shaft was measured, and the mean velocity was computed as the slope of a linear fit to the displacement data.

For the magnetostrictive-based electrohydraulic actuator, a laminated Terfenol-D rod (Chaudhuri et al., 2006, 2009) was the main driving element. Figure 9 shows an exploded view of the pumping section of the actuator. The pumping section houses the Terfenol-D rod, magnetizing coil, pump body, and piston and reed valve assembly. The pump body and bottom cap are made of high-permeability steel (12L14 grade) and act as the return path for the magnetic flux; a well-designed low-reluctance flux return path is required to complete the magnetic circuit (Butler, 1988; Giurgutiu and Rogers, 1997). The rod can be preloaded by tightening the end cap and using disk springs present within the housing; the disk springs also aid in retracting the pumping piston assembly during the *intake* stage when the active material undergoes contraction. The passive reed valves are cut out of thin spring steel sheets and then sandwiched between two steel plates in the pump head assembly to build a unidirectional fluid port (Figure 10). The pumping piston assembly consisted of a precision machined piston head and a base plate, with the metal diaphragm placed firmly in between. The motion of the Terfenol-D rod is transferred to the pumping piston using a rigid connector piece that translates within the pump top cap; this, in turn, affects the stress on the material due to variations in fluid pressure within the pumping chamber.

The ability to apply and vary the prestress on a magnetostrictive driving element is important as the

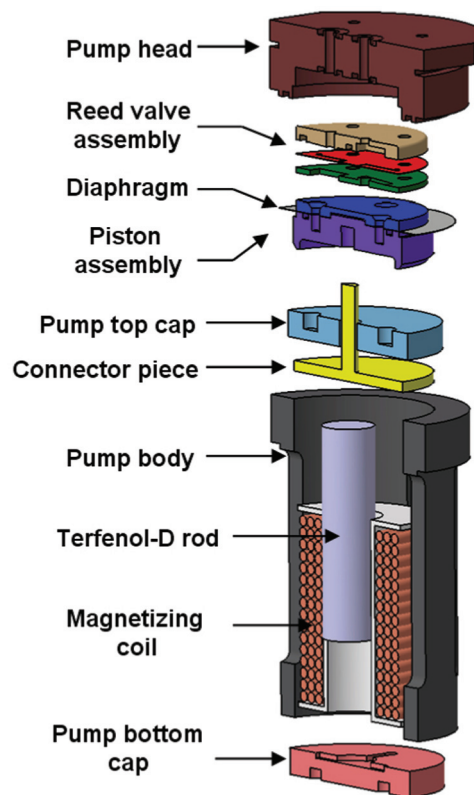


Figure 9. Exploded view of magnetostrictive-based hybrid pumping section.

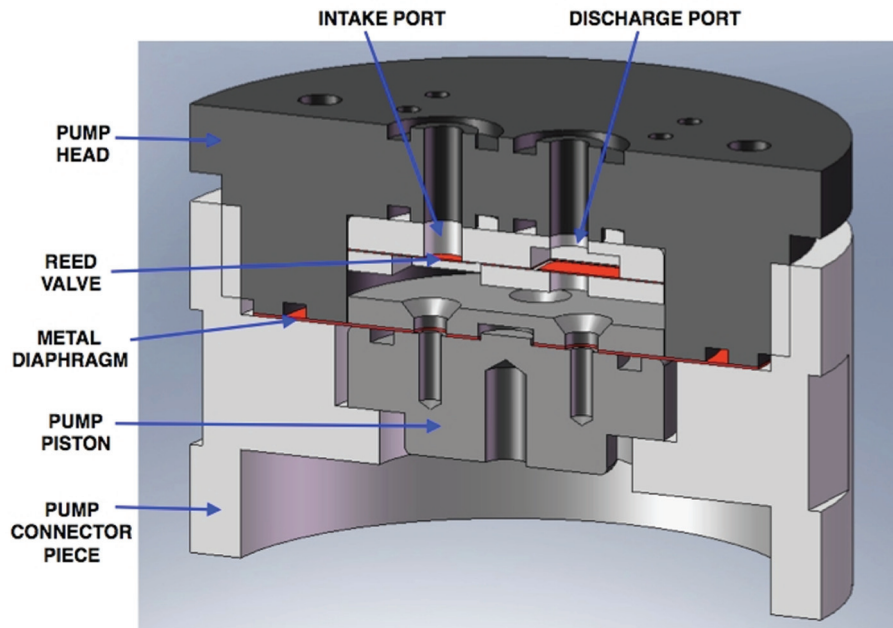


Figure 10. Hybrid pump head assembly with unidirectional discharge and intake reed ports.

magnetically induced strain, or magnetostriction, is a direct function of the prestress applied (Clark et al., 1983; Moffett et al., 1991; Calkins et al., 1997; Dapino, 2004). In this hybrid pump assembly, the prestress was controlled by three factors:

1. Tightening the bottom cap of the pump body
2. Using disk springs of varying stiffness placed in the prestress mechanism (between the connector piece and the pump top cap)
3. Bias pressure on the fluid, which directly applies a force on the rod/stack and affects the prestrain

The active material used in the electrostrictive actuator was the single-crystal electrostrictor PMN-32% PT; the stack was built from thin layers of the electrostrictive material with thin electrode layers in between. With the exception of the magnetizing coil, the remaining pump assembly is similar to the earlier description.

The hybrid pump was mated to a hydraulic cylinder *via* a manifold allowing flow from the pump to be transferred to an output device. This configuration completely separates the active material-based pump from the hydraulic subsystem and allows easy changes on either side; for example, hybrid pumps of different sizes can be connected to the same hydraulic system, or different hydraulic fluids can be used without changing the driving element.

Several physical parameters were measured during the actuator performance tests. Motion of the output shaft, measured using a linear displacement transducer, was used to calculate the output velocity. The output flow rate, which is directly proportional to the velocity

of the output, and the pressure developed in the fluidic subsystem are important parameters used to characterize a fluid pumping device. The induced strain in the active driving material was also measured using strain gages and allowed the designers to tune the mechanical impedances to achieve maximum electromechanical energy transfer. For the magnetostrictive-based actuators, the magnetic flux density through the sample can also be measured using a sense coil wrapped around the rods.

Static and Dynamic Characterization. The dynamic behavior of the material and input electrical or magnetic circuit has to be taken into consideration for modeling the performance of compact hybrid actuators at high frequencies. Such tests have also been carried out earlier to find the material properties under different driving conditions and prestress levels (Hall and Flatau, 1993; Faidley et al., 1998; Dapino et al., 2006). In tests with both the electroactive and magnetoactive elements, frequency sweeps with the active material of the pump setup without connecting the fluid circuit reveal the input response in the absence of fluid–structure coupling at the pumping piston interface.

Piezoelectric and electrostrictive materials do not show any appreciable change in induced strains with increase in signal frequency for the same applied electric fields (Sirohi et al., 2005; Nersessian et al., 2007), as depicted in Figure 11(b). A notable observation from the hysteresis behavior of PMN-PT stacks is that they are also insensitive to changes in frequency up to 1 kHz (Chaudhuri and Wereley, 2008, 2010); this uniform behavior makes the electrostrictive material more

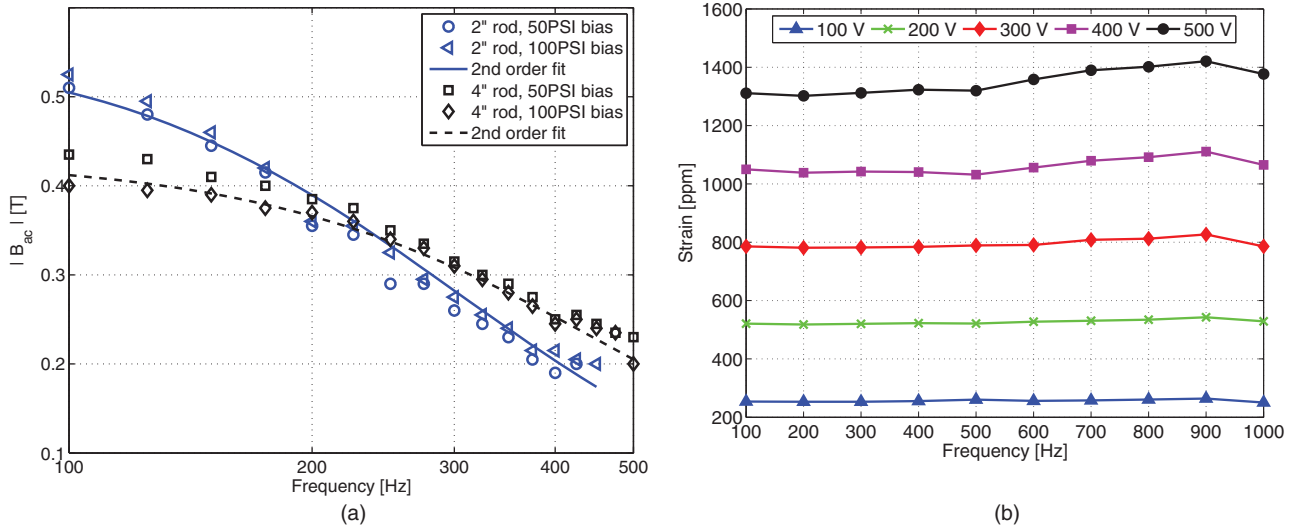


Figure 11. Induced strain behavior of prestressed smart materials at different actuation frequencies: (a) Terfenol-D rods and (b) PMN-PT stacks.

attractive than piezoceramics, the latter being prone to suffer from increasing hysteresis at high frequencies (Keoschkerjan et al., 2002; Sirohi and Chopra, 2003; Ronkanen et al., 2004).

Although the electroactive materials exhibit a capacitive effect, the presence of a magnetizing coil for magnetostrictive actuation results in low-pass behavior and limits the operational frequency range of the electrical circuit. This is clearly seen in Figure 11(a), where the induced strain in the active magnetostrictive element (of different lengths and at different axial loads) is plotted as a function of input frequency. These frequency sweeps were conducted with the prestressed material within the pump body; the fluidic subsystem was not connected. The response of the magnetostrictive material, Terfenol-D, clearly shows a drastic decrease in mechanical output that can be approximated by a second-order transfer function of the form

$$G(s) = \frac{B_{ac}(s)}{V_{in}(s)} = \frac{K_{dc}}{1 + 2\zeta(s/\omega_n) + (s/\omega_n)^2}. \quad (8)$$

Clearly, using pumping frequencies beyond a certain critical value will not lead to any performance gains (in terms of volumetric flow rate) from the overall smart pump. Artificial means of increasing frequency bandwidth are, therefore, necessary for high-frequency operation of the magnetic devices.

Actuator Performance under Free and Loaded Conditions

Tests were carried out under no-load and externally loaded conditions to measure the performance of the hybrid actuator. No-load tests, where the output cylinder shaft is allowed to move freely, provide the

maximum obtainable velocity and flow rate from the hybrid pump, whereas tests with external loads are used to determine the blocked force and power output of the actuator.

With no external loads, the hybrid actuators generally exhibit gradual increase in output shaft velocity (or volumetric fluid flow) with pumping frequency till it reached a certain peak value, after which the output drops sharply (Sirohi and Chopra, 2003; Chaudhuri et al., 2009; Chaudhuri and Wereley, 2010). This peak pumping frequency also exhibits strong dependence on fluid bias pressure; the frequency at which maximum flow rate was obtained increased with rise in fluid pressure. Although this result suggests that increasing bias pressure, and hence fluid bulk modulus, is necessary for high-frequency actuation, it does not ensure better performance; this is because a mismatch between the mechanical impedances of the driving material and the pressurized fluid chamber leads to decrease in the actual induced strain in the active material (Giurgiutiu et al., 1997). The no-load test results also show substantial reduction from initial design predictions, as the ideal, quasi-steady calculations assume maximum induced strain in the active material and do not account for any viscous, compressibility, or inertia losses in the fluidic system. The actual induced strains in the active material during pump operation have been observed to be much lower than the measurements under free conditions.

From Equations (1) and (2), it can clearly be seen that the output velocity v_L is directly proportional to the pumping frequency f under ideal conditions. However, the results of our tests indicated that the output increases only over a certain frequency range and then decreases rapidly. This phenomenon can be attributed to the following causes:

1. *Fluid inertia.* As the mass of fluid in the tubing is being accelerated in every cycle, the inertia of this volume of fluid becomes important. In the most simple case, the fluid block in the manifold resembles a SDOF system and can be associated with a resonant peak frequency, beyond which the energy required to drive the system increases exponentially. Consequently, there is a sharp drop in the movement of fluid in these sections as the frequency of operation increases and places an upper limit on the maximum frequency of operation of the pumping device.
2. *Magnetic circuit properties.* Due to the presence of a high-inductance magnetizing coil for driving magnetostrictive rods, the input circuitry behaves as a low-pass system that prevents the buildup of magnetic field in the magnetic circuit when the input signal increases and vice versa. Hence, the driving force drops with frequency, resulting in further lowering of system performance.
3. *Mechanical subsystems.* There are three mechanical subsystems that might effect the limitations of the system:
 - Flow rectification valves. The reed valves can be visualized as cantilever beams oscillating in a fluid. Although the natural frequency of the spring steel reeds vibrating in air is quite high, the presence of a dense hydraulic fluid reduces the resonant frequency drastically (Blevins, 1979). In certain cases, the modified natural frequency can lie within the range of pumping frequencies and hence be a limiting factor in the pump performance.
 - Output shaft. As the output shaft undergoes a start–stop motion in every cycle, the friction force associated becomes higher due to the stiction effect. Although the mass of the output shaft has inertial effects too, it is much lower compared to the seal friction; however, with the addition of external loads to the output cylinder, the combined inertia of the output shaft will also be of equal importance.
 - Pumping section. The natural frequency of axial vibration of the electroactive stack or magnetoactive rod placed within the pump body is also an important factor for efficient operation. Using Rayleigh's coefficient, we can approximate the modal frequency of the pumping section using the axial rigidity $EAm(x)$ and linear mass density $m(x)$ as follows:

$$\omega_r^2 = \frac{K[Y_r(L)]^2 + \int_0^L EA(x)[Y_r'(x)]^2 dx}{M[Y_r(L)]^2 + \int_0^L m(x)Y_r^2(x) dx}, \quad (9)$$

where M is the end mass, K is the stiffness of the disk spring(s) used for prestressing, and L is the overall length of the rod. The end mass consists of the prestress connector and flux return pieces. Usually, this value is much higher but can be of concern at very high pumping frequencies.

The procedure for tests with external loads is similar to unidirectional no-load testing, with the addition of measured weights from the end of the vertically oriented output cylinder shaft. Maintaining constant load, the pumping frequency is increased till the motion of the actuator is negligible; this gives a measure of blocked load for a particular pumping frequency. Information obtained from force–velocity diagrams is used to calculate the maximum obtainable power output from the device. As the actuator works on the basis of frequency rectification, the maximum power that can be obtained from the system is the area of the biggest rectangle that can be enclosed inside the linear load line (Sirohi and Chopra, 2003; John et al., 2007, 2008). Thus, maximum power output, P_{out} , is half the area enclosed under the load line, that is,

$$P_{out} = \frac{1}{4} \times F_{block} \times v_{no-load}, \quad (10)$$

where F_{block} is the blocked force and $v_{no-load}$ is the maximum output velocity (under no-load conditions) of the actuator.

During the tests, the output velocity of the actuator dropped sharply when an external load was applied. This was also accompanied by a shift in the peak frequency to lower values (Sirohi and Chopra, 2003; Chaudhuri and Wereley, 2010), which was expected because the addition of inertial load mass effectively lowers natural frequency.

MRFs for Bidirectional Operation

By itself, the unidirectional flow from the hybrid pump can only produce unidirectional motion of the load. To produce bidirectional motion, we have to introduce a valve system between the pump and the output cylinder that switches the direction of fluid flow depending on the desired direction of motion of the output.

Previous studies (Yoo and Wereley, 2004) have shown the feasibility of using MRF-based valves to produce the bidirectional motion of the output cylinder shaft. MRFs are a kind of semiactive smart materials, where the rheological behavior of the fluid can be altered by applying a magnetic field (Phulé, 2001); this controllable action has found applications in several fields in recent times (Carlson and Jolly, 2000).

The MR valves used by Yoo and Wereley (2002) consist of a core, a flux return path, and an annulus through which MRF flows. The core is wound using insulated copper wire, and current is passed through

this coil to create a magnetic field at the active section. The MRF in the active section encounters the magnetic field and its rheological properties change, giving rise to a yield force; flow is initiated only if the pressure difference is greater than the yield stress. This blocking property enables us to use MRFs in fluidic valves.

The schematic of the MRF valve network is shown in Figure 12. The network consists of four MR valves arranged in a H-bridge configuration with an accumulator at the low-pressure side of the pump and a conventional hydraulic cylinder to obtain output motion (Yoo and Wereley, 2002, 2004). A commercially available double-acting hydraulic cylinder can be used for output motion. By applying a magnetic field to valves 2 and 4, the resulting fluid flow from the pump can be prevented from flowing through valves 2 and 4 and forced to flow only through valves 1 and 3, thus pushing the output cylinder shaft upward (Figure 12(a)). If, however, we apply a magnetic field to valves 1 and 3, the fluid is allowed to flow only through valves 2 and 4, thus pushing the cylinder shaft downward (Figure 12(b)). Some of the reasons for the low performance were (1) leakage through MR valves due to finite yield stress, (2) denser transmission fluid, and (3) higher viscous losses.

System Model

Theoretical modeling of the hybrid system is extremely complex and several models have been proposed in literature. Models based on stiffness matching of the actuator stack with an incompressible fluid under static

conditions were used for preliminary design and work output of piezoelectric-based devices (Liang et al., 1994, 1996, 1997; Giurgiutiu and Rogers, 1997; Giurgiutiu et al., 1997; Mauck and Lynch, 2000; Nasser and Leo, 2000; Sirohi and Chopra, 2003; Heverly et al., 2004). Although these formulations were useful for a first-hand understanding of the device physics and to estimate operational efficiency, the complete operation of the coupled electrohydraulic actuator could only be modeled by more comprehensive schemes, some of which are listed in the following. In recent times, CFD has also been used in some studies to derive loss coefficients for flow in and out of the pumping chamber (Oates and Lynch, 2001; John et al., 2006, 2009). However, these computations are very specific to the geometry and size of the control volume and the flow path.

Static and Quasi-Static Models

The earliest models for hybrid hydraulic actuators were derived from idealized assumptions. Calculations based on stiffness matching of the actuator stack with an incompressible fluid were used for preliminary design and efficiency calculations of piezoelectric-based devices (Giurgiutiu et al., 1995; Giurgiutiu and Pomirleanu, 2001).

In the piezohydraulic pumping theory developed by Mauck and Lynch (2000), a piezoelectric stack actuator provided the mechanical driving force for actuation of the pump. The maximum work was obtained from a stack actuator when it was impedance matched to the

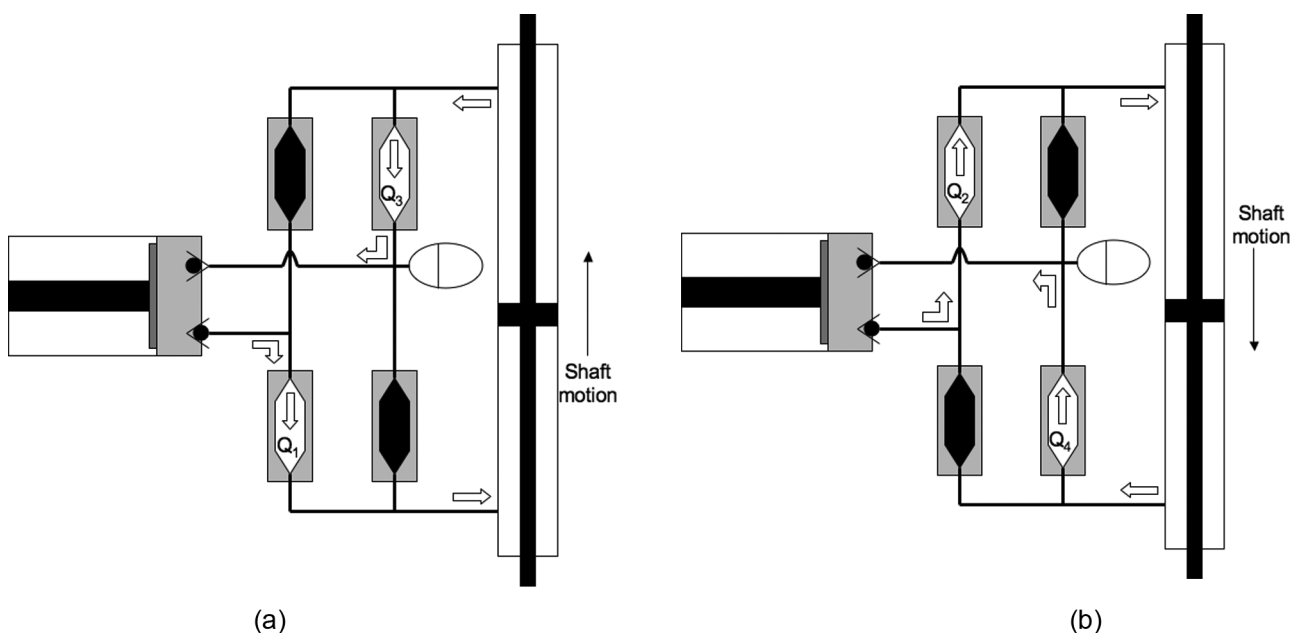


Figure 12. Schematic for the active modes of the MR-based bidirectional actuation system: (a) upward motion and (b) downward motion.

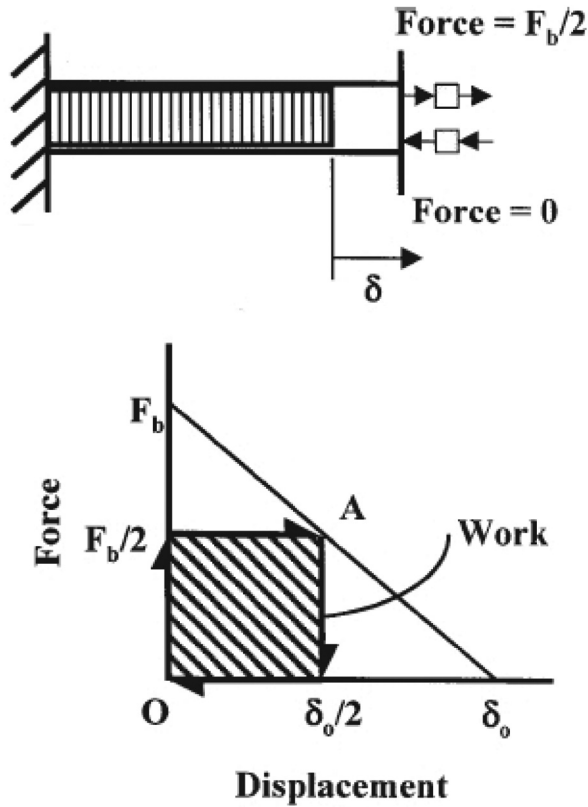


Figure 13. Work cycle for an impedance-matched stack actuator.

load it was driving. Figure 13 shows the work cycle for an impedance-matched PZT stack in a pump cycle where the outlet check valve opens at a pressure corresponding to $F_b/2$ on the loading half of the cycle, and the inlet valve opens at a pressure corresponding to zero on the unloading half of the cycle. Correspondingly, the work done on the loading half of the cycle is the shaded area under the curve, that is,

$$W = \frac{1}{2} \left(\frac{F_b}{2} \right) \left(\frac{\delta_o}{2} \right).$$

The model developed by Sirohi and Chopra (2003) was based on the force–displacement characteristics of the smart material, as shown in Figure 14. The equation of the piezostack load line was given by

$$\delta = \delta_{free} \left(1 - \frac{F_o}{F_{block}} \right),$$

where δ_{free} and F_{block} are properties of the piezostack. Also, the displacement of the active stack is obtained by representing the stack and fluid column as stiffnesses K_p and K_f , respectively:

$$\delta_o = \delta_{free} - F_o \left[\frac{1}{K_p} + \frac{1}{K_f} \right], \quad K_f = \beta \frac{A_p}{\Delta_{gap}}.$$

The pumping chamber has a cross-sectional area A_p and a displacement δ_p , whereas the output actuator has a cross-sectional area A_{out} and a displacement δ_{out} . Writing the area ratio as $A_R = A_{out}/A_p$, the output force F_{out} is related to the actuator force F_o by

$$\frac{F_o}{A_p} = \frac{F_{out}}{A_{out}} \Rightarrow F_o = \frac{F_{out}}{A_R}.$$

The work done per cycle is

$$\Delta W_{cyc} = F_o \delta_o = F_o \left(\delta_{free} - \frac{F_o}{K_{eff}} \right), \quad K_{eff} = \left(\frac{1}{K_p} + \frac{1}{K_f} \right)^{-1}.$$

Writing this in terms of output force, the output work could be obtained from

$$\Delta W_{cyc} = \frac{F_{out}}{A_R} \left(\delta_{free} - \frac{F_{out}}{A_R K_{eff}} \right).$$

To include effects of the active check valves used for rectification of the flow, a flow factor, C_f was defined to relate the volumetric flow rate, Q , to the differential pressure, ΔP , across the valve by the expression (Sirohi, 2002)

$$Q = C_f \sqrt{\Delta P}, \quad \Delta P = P_{ch} - P_o,$$

where P_{ch} and P_o are the pressures in the chamber and the output tubing. If the inlet valve is open, the pumping chamber would be connected to the low-pressure accumulator and $P_o = P_{low}$. Similarly, if the outlet valve is open, the pumping chamber would be connected to the high-pressure accumulator and $P_o = P_{high}$. It was assumed that only one of the valves could be open at any given point in time. Consequently, the flow rate was calculated from the pressure drop and flow direction using

$$Q = C_f \sqrt{|P_{ch} - P_o|} \text{sgn}(P_{ch} - P_o).$$

The check valves were modeled by a cracking pressure, P_{crack} , and a hysteresis pressure, P_{hys} , that defined the conditions under which they open or close. The inlet valve was considered open when either of the following two conditions was met:

$$\begin{aligned} &P_{ch} < (P_{low} - P_{crack}) \\ &\text{OR} \\ &P_{ch} < (P_{low} - P_{crack} + P_{hys}) \quad \text{AND} \quad \frac{dP_{ch}}{dt} > 0 \end{aligned}$$

Similarly, the outlet valve was considered open if

$$\begin{aligned} &P_{ch} > (P_{high} + P_{crack}) \\ &\text{OR} \\ &P_{ch} > (P_{high} + P_{crack} - P_{hys}) \quad \text{AND} \quad \frac{dP_{ch}}{dt} < 0 \end{aligned}$$

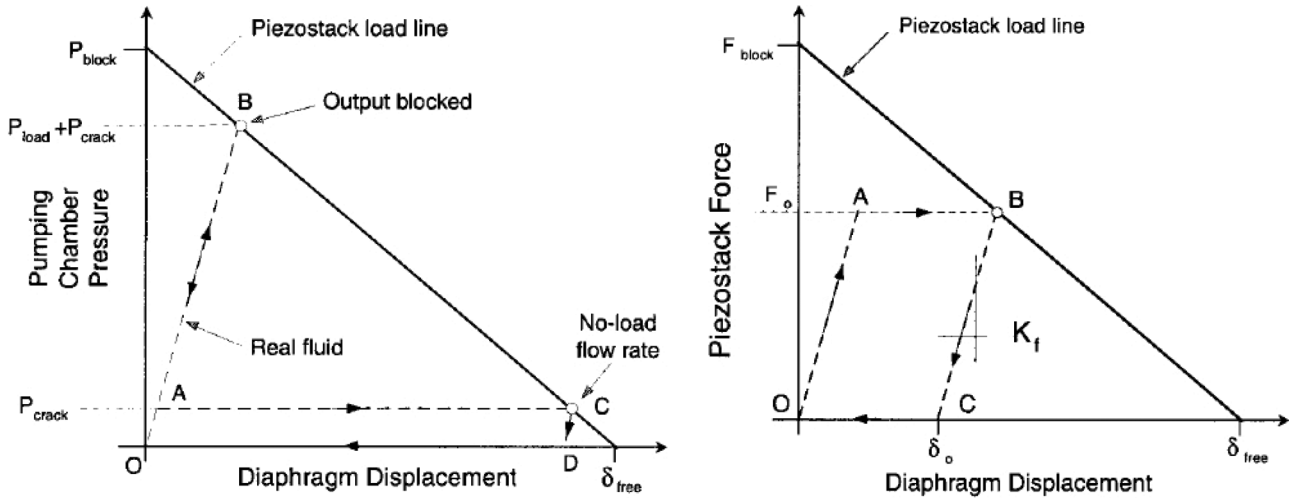


Figure 14. Load-line analysis for a piezoelectric actuator (Sirohi and Chopra, 2003).

Although this analysis did not assume any dynamics of the valve itself, the flow factor was related to the pressure difference by

$$C_f = \begin{cases} 0 & \text{if } \Delta P < P_{crack} \\ \frac{\Delta P - P_{crack}}{P_{full} - P_{crack}} C_{f0} & \text{if } P_{crack} \leq \Delta P < P_{full} \\ 1 & \text{if } \Delta P \geq P_{full} \end{cases}$$

where C_{f0} is the flow factor when the valve was fully open with a differential pressure higher than P_{full} .

Lindler et al. (2003) calculated the operational efficiency starting from elementary considerations that took into account the compressibility of the chamber fluid and pressure drop in the valves. The maximum work output per cycle (time period T) was obtained from the blocked force F_b and free displacement δ_m on

the actuator load line shown in Figure 15 and was written as follows:

$$W_{max} = \frac{F_b \delta_m}{4T} = \frac{P_s \Delta V_m}{4TA^2},$$

where P_s was the stall pressure and ΔV_m was the maximum volume displacement. By including the viscous pressure loss P_v in the valves, the work output was written as follows:

$$W_{out} = \frac{(P_s - P_v)A}{4T} \left[\delta_m - \beta P_s \frac{V}{A} \right].$$

A quasi-static two-stage hybrid actuator model was developed by Cadou and Zhang (2003); the intermittent opening and closing of the check valves was assumed to produce impulsively accelerated flow through the fluid tubing, and the corresponding velocity profile was used to calculate viscous losses. The authors also noted that actuation occurs in two steps during each pumping cycle; the first step is associated with pump discharge, whereas the second is associated with pump intake. The intermittent opening and closing of the check valves means that the pressure gradient that accelerates the fluid in the connecting tube is applied impulsively. As the piezostack is energized, the pressure-displacement characteristic of the stack, shown in Figure 16, sweeps upward along the pressure-displacement characteristic associated with the fluid in the pumping chamber. Viscous and inertial forces increase the effective load on the piezostack further reducing the displacement per stroke and hence the actuation velocity. This explains the tendency of the actuation velocity to roll-off at high frequencies as viscous and inertial forces increase rapidly (and nonlinearly) with operating frequency.

Assuming that the fluid is incompressible and that the velocity profile develops uniformly along the length of the tube, a closed-form expression for the fluid

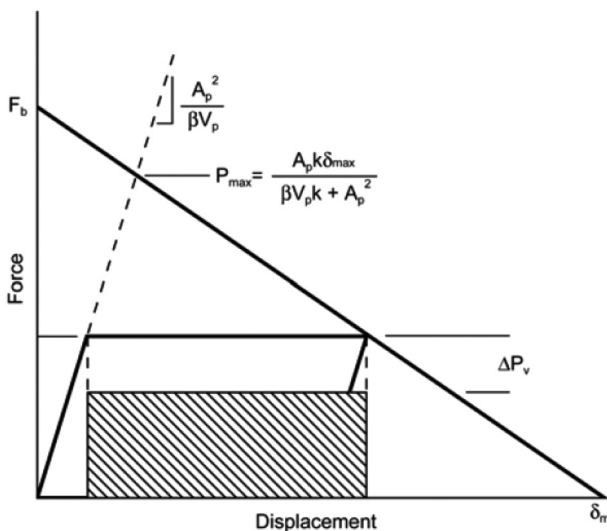


Figure 15. Load-line explanation of hybrid-actuator work showing loss elements.

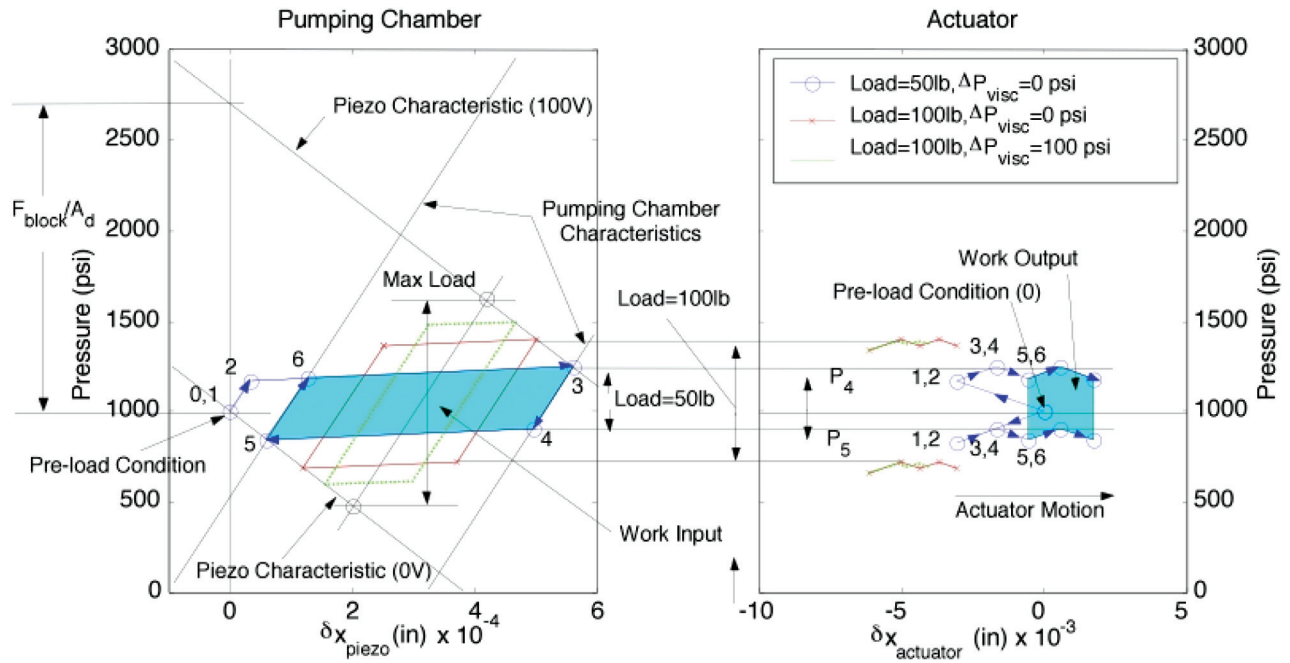


Figure 16. Illustration of pumping and stepwise actuation cycle.

velocity response u to an impulsively applied pressure gradient was obtained following Szymanski and co-workers' solution (Szymanski, 1932; Uchida, 1956; Das and Arakeri, 2000):

$$u(x, y) = \frac{h}{4} \left[x^2 - 1 - 8 \sum_{n=1}^{\infty} \left(\frac{J_1(a_n x)}{a_n^3 J_1'(a_n)} e^{-a_n^2 y} \right) \right], \quad (11)$$

where h and the nondimensional parameters x, y , were defined as follows:

$$\begin{aligned} x &= \frac{r}{R} \\ y &= \frac{\mu t}{\rho R^2} \\ h &= \frac{R^2 \Delta P_{tube}}{\mu L} = 4U_{max} \end{aligned}$$

In these expressions, R is the tube radius, ρ is the density, ΔP_{tube} is the fluid pressure drop along the tube, and L is the length of the tube. x and y are the nondimensional radial position and time, respectively. The first two terms in Equation (11) correspond to steady-state Poiseuille flow, while the unsteady component of the velocity field is represented by the third term: a series expansion in first-order Bessel functions $J(x)$ with coefficients a_n chosen such that the solution converges to the steady Poiseuille flow solution as $t \rightarrow \infty$. The product of density and velocity over the tube cross-sectional area and the valve opening time t_{open} gave the mass moved per piezo stroke, whereas the mass moved per stroke times the frequency gave the overall mass

flow rate of the system. Viscous losses were neglected in all of the components except the valves and the tube connecting the open valve with the actuator. The pressure drop across the valve was estimated using the standard assumption that the mass flow rate through the passive check valves is proportional to the square root of the pressure drop through the valve as follows:

$$\dot{m} = C_v \sqrt{\Delta P_{valve}}, \quad (12)$$

where C_v is the flow coefficient for the valve. The small cracking pressure and inertia of the valve were not included in this analysis. The system model was then built up by balancing pressures associated with each component in terms of its volume and mass and at the interface with each component, and conservation of mass in the overall system. This led to two sets of equations, one for the discharge stroke and one for the intake stroke, which were formulated in state-space and solved. Although this model did not formally address the dynamic behavior of the fluid system, the quasi-static approximation did a reasonably good job of predicting actuator performance at frequencies below 150 Hz.

Dynamic Actuator Models in Frequency Domain

A dynamic model to find the induced strain of a stacked actuator shown in Figure 17 was developed by Tang et al. (1997). The model started by considering the total energy per unit volume as follows:

$$P_v = \frac{1}{2} \sigma^T \mathbf{S}^E \sigma + \frac{1}{2} \mathbf{E}^T \mathbf{C}^{\eta} \mathbf{E} - \frac{1}{2} \mathbf{E}^T \mathbf{C}^{\eta} \mathbf{E},$$

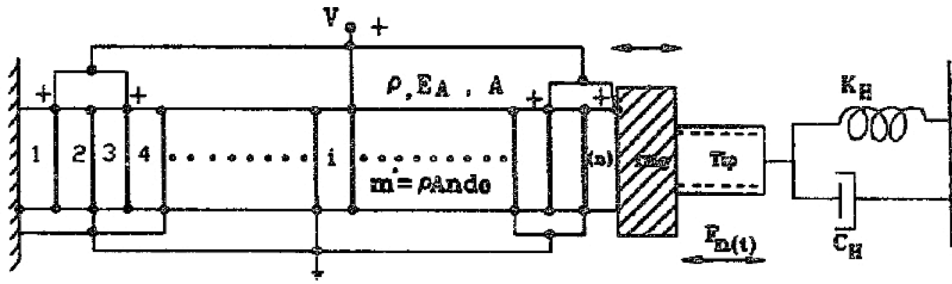


Figure 17. Model of piezoelectric actuator for dynamic analysis with tip stiffness (Tang et al., 1997).

where $V_v = (1/2)\sigma^T S^E \sigma$ is the mechanical energy density, $W_v = (1/2)\mathbf{E}^T \mathbf{C}^\eta \mathbf{E}$ is the electric energy density, and $Z_v = (1/2)\mathbf{E}^T \mathbf{C}^\eta \mathbf{E}$ is the electromechanical energy density.

For the i th thin piezoelectric ceramic plate or disk of thickness d_{0i} in the overall stack, the stress σ_i can be related to the displacement u'_i by

$$\sigma_i = E_A u'_i(x, t), \quad \text{where} \quad u'_i(x, t) = \frac{\partial u_i(x, t)}{\partial x}$$

and the corresponding elastic, electric, electromechanical, and kinetic energies were written as follows:

$$V_{Ti} = \int_{x_i}^{x_i + d_{0i}} \frac{1}{2} E_{Ai} A_i (u'_i(x, t))^2 dx.$$

$$W_{Ti} = \frac{1}{2} \frac{q_i^2}{c_i(dx_i + u_i(x_i + dx_i, t))} = \frac{1}{2} \frac{q_i^2}{c_i dx_i}.$$

$$Z_{Ti} = -d_{33i} E_i E_{Ai} A_i \int_{x_i}^{x_i + d_{0i}} u'_i(x, t) d\Omega.$$

$$T_{Ti} = \frac{1}{2} \int_{x_i}^{x_i + d_{0i}} \rho_i A_i \dot{u}_i^2(x, t) dx.$$

Assuming a stack with uniform density ρ , cross-sectional area A , and elastic modulus E_A . Correspondingly, the total energies

$$V_T = \frac{1}{2} E_A A \int_0^{nd_0} (u'(x, t))^2 dx$$

$$T_T = \frac{1}{2} \rho A \int_0^{nd_0} \dot{u}^2 + \frac{1}{2} m_e \dot{u}^2(nd_0, t)$$

$$Z_T = -d_{33} E_A A \sum_{i=1}^n \frac{q_i}{c_i d_0} \int_{(i-1)d_0}^{id_0} u'(x, t) dx$$

can be used to write the Lagrangian

$$L = T_T - V_T - W_T - Z_T$$

and the virtual work is

$$\delta W = -(-K_H - C_H \dot{u}(x, t)) \delta u(x, t)|_{x=nd_0} + \sum_{i=1}^n V_i \delta q_i.$$

This was used to derive the mode shapes and displacement of the complete stack under the application of an electric field. The transfer functions between relating the output force $F_{out}(s)$ and displacement $X_{out}(s)$ to the input force $F_{in}(s)$ and stack displacement $X_{in}(s)$ were found from tests where measurement probes were present within the setup; the input probe was used in sensing the input piston displacement through a extension bar, whereas the output piston probe was used directly to measure output displacement.

Hom and Shankar (1999) developed a dynamic model where the electrostrictive driver is a multilayered rod of total length L , cross-sectional area A , and N layers of the ceramic, represented in Figure 18. The actuator is mechanically grounded on one end and attached to a structure on the other end. The surrounding structure is mechanically represented by a complex impedance Z and a static stiffness K . The force boundary condition at the end of the rod requires

$$AT|_{x=L} = -K(u_0 + \Delta) - \sum_{\omega} Z(\omega)v(\omega),$$

where T is the stress in the rod, v is the velocity spectrum of the rod's end, and u_0 is the static displacement of the rod's end, and Δ is the mismatch between the

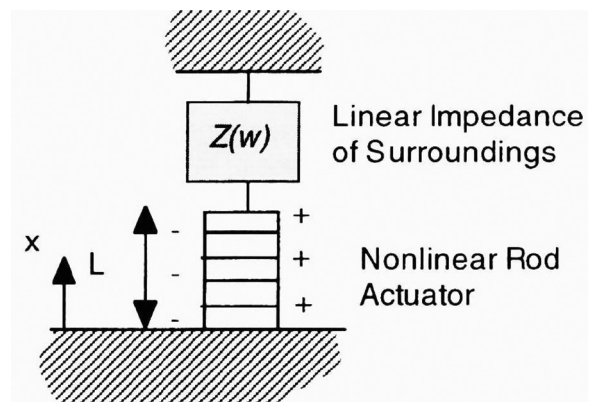


Figure 18. Model of mechanical system driven by a multilayered electrostrictive actuator.

actuator and the structure. The ceramic's electromechanical behavior was modeled with the 1D electrostrictive constitutive law developed earlier by the authors (Hom and Shankar, 1994) and consists of the following coupled mechanical and electrical equations

$$S = s_{33}T + Q_{33}P^2$$

$$E = -Q_{33}PT + \frac{1}{k} \operatorname{arctanh}\left(\frac{P}{P_s}\right),$$

where S is the longitudinal strain, P is the polarization, and E is the applied electric field; Q_{33} , the longitudinal electrostrictive coefficient; P_s , the saturation polarization; and k , a new material constant, must be measured experimentally from electrical tests without prestress.

A dynamic system model that coupled the piezoelectric stack actuator with the mechanical and fluid compliances and the viscous effects of the working fluid was developed by Oates and Lynch (2001) using a state-space analysis. Equations of motions of the electromechanical and fluid subsystems were derived. The stack actuator/piston subsystem was modeled as a second-order mass-spring-damper with a driving force provided by an input voltage. The stack itself was modeled as a spring (stiffness k_1) in series with a displacement producing actuator (x_1) that was extended by a voltage input (V). The voltage input was converted to mechanical displacement of a stack actuator using the constitutive law of the piezoelectric material. This provided a driving force to the piston mass m_p on the actuating side. A second force on the right-hand side of the piston was generated by the fluid pressure in the cylinder head (P_1) applied to the piston area (A_{pi}). The friction associated with the o-ring and fluid between the piston and cylinder walls was represented by a viscous damping coefficient, b_p . The resulting equation of motion for the stack actuator/piston assembly is

$$m_p \ddot{x}_1 + b_p \dot{x}_1 + k_1 x_1 = cV - P_1 A_{pi},$$

where the constants c and k_1 were derived from the linear constitutive law of the piezoelectric material.

$$S_{33} = s_{3333}^E T_{33} + d_{333} E_3,$$

where S_{33} is the axial strain component, T_{33} is the axial stress component, E_3 is electric field component, s_{3333}^E is the compliance component at fixed electric field, and d_{333} is the piezoelectric coefficient in this formulation. The stress and electric field were applied in the uniaxial direction. In terms of force (F), displacement (x_1), and voltage (V), this becomes

$$F = \frac{nA_{PZT}Ed_{333}}{L} V - \frac{A_{PZT}E}{L} x_1.$$

The spring constant, k_1 , is equivalent to $\frac{A_{PZT}E}{L}$ and was based on the effective modulus and geometry of the stack actuator. The piston in the hydraulic actuator was modeled as a mass and damper in parallel, with the o-ring and fluid friction represented by the damping.

The flow resistance through the rectifying check valves was modeled as a finite resistance in one direction and an infinite resistance in the opposing direction. Lumped parameter fluid subsystems were developed for coupling the fluid dynamics with the electromechanical subsystems. Equations of mass continuity and definition of bulk modulus were used to develop the fluid dynamic equations as follows:

$$\dot{m}_{in} - \dot{m}_{out} = \frac{d(\rho V)}{dt}$$

$$\beta_e = \rho_0 \frac{dP}{d\rho}$$

$$\frac{\rho_0 V_0}{\beta_e} \dot{P} = C \dot{P} = \sum_{i=1}^n \dot{m}_i = \frac{\Delta P}{R}$$

Mass flow was represented by m_i , and the pressure and rate of pressure change were ΔP and \dot{P} , respectively. Capacitance (C) values were calculated for each control volume within the pump system. The effective bulk modulus ($\beta_e = 70$ MPa) of the system used by Oates and Lynch was two orders of magnitude lower than the fluid bulk modulus specified by the manufacturer; this reduction in stiffness was attributed to the presence of o-rings and entrained air in the system.

A different approach was applied by Ullmann and co-workers (Ullmann et al., 2001; Ullmann and Fono, 2002) to the valveless piezopump system, where a sinusoidal force was assumed to drive the fluidic systems and the natural frequency of the pumping system was calculated; pressure drops in different sections of the pump were well represented in these formulations. The driving voltage supplied to the piezoelectric device was assumed to be converted into periodic force acting on the center of the disk, whose elasticity was simulated by a spring with a spring constant. The fluid was considered to be incompressible, and its inertia was included in force balance equations for different sections of the pipes. For the outlet pipe section with cross-sectional area A_p and at pressure P_1 , force balance yielded

$$P_1 A_p = P_{out} A_p + m_p \ddot{x}_p + \frac{32\mu L_p}{D_p^2} \dot{x}_p A_p,$$

whereas the nozzle section, of cross-sectional area A_n , was represented by

$$P_2 A_p = P_1 A_p + m_n \ddot{x}_n + \frac{1}{2} K_L \dot{x}_n A_n,$$

where x_p and x_n are the mean displacements of the fluid in the pipe and nozzle, respectively. On the right-hand side of both equations, the second term represents the fluid inertia, while the third term represents the viscous losses. For the pipe, the viscous losses were calculated

assuming laminar flow, whereas an empirical constant K_L was used for the squared losses in the nozzle. The fluid was assumed to be incompressible, hence, by applying the continuity equation:

$$\dot{x}_p = \frac{A_n}{A_p} \dot{x}_n \quad \text{and} \quad \ddot{x}_p = \frac{A_n}{A_p} \ddot{x}_n.$$

Using these relations, the two force balance equations were combined to obtain a single governing ordinary differential equation (ODE) for the mass flow rate out of the pump. A similar formulation was used for the inlet line and nozzle. Finally, the force balance on the piezoelectric membrane, which contained the piezoelectric element and supporting disk, resulted in

$$K_D m_D \ddot{x} = F \sin(\omega t) - Kx - A_D K_P P_3,$$

where F is the amplitude of the force acting on the center of the disk, K is the equivalent spring constant, K_D is a correction factor that takes into account that not all of the parts of the membrane are displaced as the center (x), and K_P is a correction factor that converts the continuous force (due to pressure difference) that acts on the membrane into a fictitious force acting centrally.

Nasser and Leo (2000) developed a lumped parameter-based dynamic model for the hydraulic and active components of the systems by linearizing the nonlinear behavior of the fluid and using the resulting variables to calculate work done and output efficiency of the device. The operation of the hybrid pump was broken up into four distinct regimes as shown in Figure 19, along with rectification by a set of unidirectional valves.

Work and energy expressions were derived from a 1D model of a piezoelectric actuator. Overall system efficiency of the device was calculated for two different scenarios. An idealized model of incompressible fluid illustrated that the mechanical efficiency of the rectification process is 100%, but the electrical efficiency varied between 5% and 29% depending on the actuator coupling coefficient. The mechanical efficiency was between 4% and 40% when using compressible gas as the transmission media, whereas the electrical efficiency of the process was between 1% and 7% for this process.

Fluid transfer matrix models were used by Sirohi et al. (2003, 2005) to obtain a frequency-domain model of the pump operation. Starting from the basic fluid equations of continuity, momentum, and energy, the relation between the pressure, P , and volume flow rate variables, V , at the ends of the fluid line can be derived in terms of a transfer matrix as follows:

$$\begin{Bmatrix} P_1 \\ Q_1 \end{Bmatrix} = T_{12} \begin{Bmatrix} P_2 \\ Q_2 \end{Bmatrix} \quad (13)$$

where

$$T_{12} = \begin{bmatrix} \cosh \Gamma & -Z_c \sinh \Gamma \\ -\frac{1}{Z_c} \sinh \Gamma & \cosh \Gamma \end{bmatrix}.$$

This is a standard representation used in hydraulic analyses, where the assumptions are

- Fluid velocity is lower than acoustic velocity
- Laminar flow in a rigid tube of circular cross section

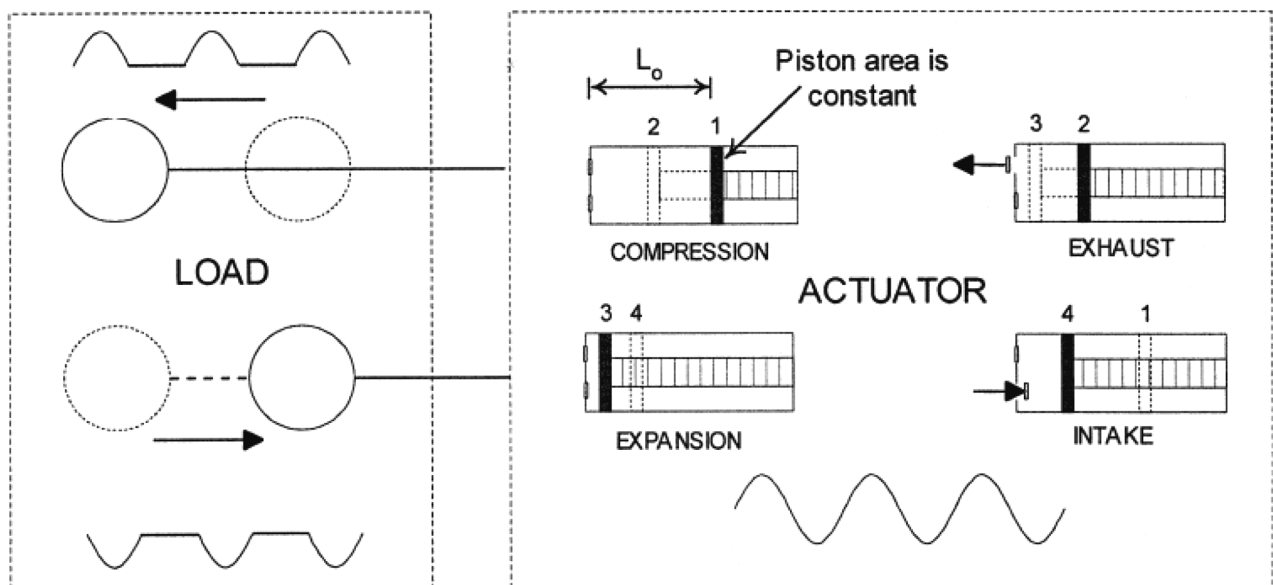


Figure 19. Frequency rectification concept using piezoelectric actuation.

- Length of tube is larger than the diameter ($l/r \gg 1$)
- Normalized density variations are small ($\Delta\rho/\rho \ll 1$)

The behavior of the fluid line is governed by two quantities, the characteristic impedance Z_c and the propagation parameter Γ , both of which can be calculated from density and bulk modulus of the fluid. The complete model was then built by connecting the fluid matrices with SDOF matrices of piston motion, which was achieved in frequency domain by simple multiplication of corresponding transfer matrices. The frequency response of the device was calculated by assuming a harmonic excitation at a frequency ω . The accumulator was treated as a section of tubing with a local compliance much higher than the surrounding fluid. Such an approximation resulted in a constant pressure across the accumulator, and a difference in the flow rate upstream and downstream of the accumulator. Force equilibrium on the piezostack was used to obtain the governing equation:

$$c_v - P_c a_p = m_p \ddot{x}_p + b_p \dot{x}_p + k_p x_p,$$

where P_c denoted the pressure in the pumping chamber. Assuming the output mechanical load to be lumped together with the output piston, force equilibrium on the output piston yielded

$$(P_{lp} - P_{up})A_o = m_o \ddot{x}_o + b_o \dot{x}_o + k_o x_o,$$

where x_o is the output displacement. The pressure drops at the check valves are linearly related to the volume flow rates:

$$\begin{aligned} \text{Exhaust : } P_c - P_1 &= R_{out} Q_1 \\ \text{Intake : } P_4 - P_c &= R_{in} Q_4 \end{aligned}$$

Using the state vector $\mathbf{q} = [x_p \ x_o \ P_c \ P_1 \ P_4 \ P_{lp} \ P_{up}]$, the above linear equations were combined and written in simple form as follows:

$$\mathbf{M}\ddot{\mathbf{q}} + \mathbf{C}\dot{\mathbf{q}} + \mathbf{K}\mathbf{q} = \mathbf{F}.$$

The analysis correlated well with the measured results for frequencies below the first natural frequency of the system, which could be predicted with an accuracy of 10%–15%. The authors attributed discrepancies between theory and analysis to significant nonlinearities in the system, such as static friction in the rod seals and piezostack frequency response on the magnitude of actuation voltage.

Rupinsky and Dapino (2006) further extended this formulation to include a transduction model for electromechanical coupling using the equations

$$\begin{aligned} V &= Z_e I + T_{em} v_t \\ F &= T_{em} I + Z_m v_t, \end{aligned} \quad (14)$$

where V is the applied voltage to the transducer; I is the current flow through the transducer; F is the force on the transducer; v_t is the velocity; Z_e and Z_m are the blocked electrical and mechanical impedances, respectively; and T_{em} and T_{me} are transduction coefficients that describe the electromechanical coupling. The coefficients were calculated from actual mechanical and electrical properties of the material, which, in case of a magnetostrictive material, are analogous to coefficients of the linear piezomagnetic constitutive relations combining the elastic and magnetic effects on the strain ϵ and magnetic induction B :

$$\begin{aligned} \epsilon &= s^H \sigma + d_a H \\ B &= d_a^* \sigma + \mu^\sigma H, \end{aligned} \quad (15)$$

where σ is the stress on the Terfenol-D rod, H is the magnetic field through the rod, s^H is the elastic compliance at constant magnetic field, $d_a = d_a^*$ are piezomagnetic coupling coefficients, and μ^σ is the magnetic permeability at constant stress.

Dynamic Actuator Models in Time Domain

Models for hybrid pumps formulated in time domain and taking into consideration fluid compressibility and inertial elements exist in literature. Nasser and co-workers (Nasser, 2000; Nasser et al., 2001) developed a dynamic model of a piezohydraulic pump by considering both inertia and compressibility of the transmission fluid along with the linearized equations for a smart piezostack. A lumped parameter approach was applied to the fluid system, which was then solved using an electrical network analogy. The resistance, capacitance, and inductance were defined and related to the mechanical variables as follows:

$$\begin{aligned} \text{Resistance : } R_f &= \frac{128\mu l}{\pi D^4} \left(1 + D \sum (l/d)_{eq}\right) \sim b \\ \text{Capacitance : } C_f &= \frac{A l}{\beta} \sim \frac{1}{k} \\ \text{Inductance : } I_f &= \frac{\rho l}{A} \sim m \end{aligned}$$

Using these, the pressure drop through any lump with flow rate Q was written as:

$$\Delta P = R_f Q + I_f \frac{dQ}{dt} \equiv \Delta V = RI + L \frac{dI}{dt}.$$

where the current I is equivalent to the flow rate in the analogous electrical circuit. The compliance C_f was added to the electrical network using a capacitor C , thereby arriving at the overall expression by considering a current source (flow rate), as depicted in Figure 20:

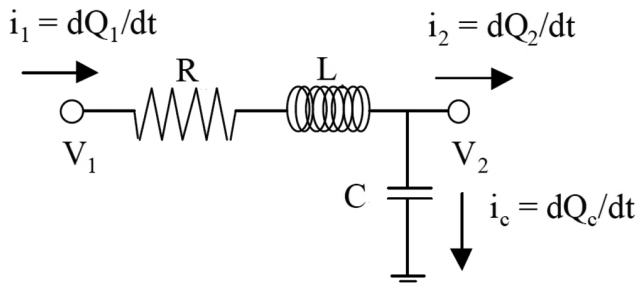


Figure 20. Lumped parameter fluid mode using electrical network analogy.

$$L \frac{d^2 Q_1}{dt^2} + \frac{1}{C} (Q_1 - Q_2) + R_1 \frac{dQ_1}{dt} = 0.$$

The lumped parameter approach was extended to the pumping stack, the end effector, and the fluid volumes on the input and output sides of the hydraulic cylinder, resulting in force balance ODEs for all cases. The model was seen to work well in the case of one-sided operation for frequencies up to 100 Hz. When the action of the active valves was included in the simulation by incorporating valve timing, the model captured the pump behavior up to 8 Hz. One of the problems noted was due to time lag in cylinder motion whenever the frequency of valve operation was increased, possibly caused by the inertia of the fluid. The authors noted that a model of the valves should include reverse motion for more accurate representation.

Regelbrugge et al. (2003) derived a simple, physics-based model to describe basic operating characteristics of piezohydraulic actuators. The bulk modulus of the hydraulic fluid along with mass flow rates through different control volumes were used to calculate the pressures in the corresponding sections of the actuator. The input was assumed to be sinusoidal displacement of the piston driven by a piezoelectric stack. Motion of the mechanical components and fluid volumes were modeled using SDOF equations from dynamic force equilibrium considerations. Pressure drops through the valve orifices connecting volume elements were modeled using a momentum-conserving relation (Bernoulli's equation) with empirical corrections for viscous flow losses and jet contraction; the mass flow rate through a valve, \dot{M} , was calculated as a function of the pressure difference, ΔP , across it as follows:

$$\dot{M} = \frac{2A}{2 + \pi} \operatorname{sgn}(\Delta P) \sqrt{2\rho(\Delta P - P_v)}, \quad (16)$$

where ρ is the instantaneous density of the fluid in the valve, A is the valve opening area, and P_v is the viscous pressure loss in the valve. The model progresses between time steps using the governing ODEs and kept track of the mass of fluid, M , in each section using the relation:

$$M = \rho(V - Ax). \quad (17)$$

where V is the volume and x is the displacement of a boundary. The bulk modulus of the fluid was used to calculate the pressure in any fluid volume based on the instantaneous density in the same volume from the following relation:

$$\begin{aligned} dP &= -\beta \frac{dV}{V} = \beta \frac{d\rho}{\rho} \\ \Rightarrow P - P_0 &= \beta \ln\left(\frac{\rho}{\rho_0}\right). \end{aligned}$$

A similar approach was used by Tan and co-workers (Tan, 2002; Tan et al., 2005); in addition to the losses in valves, this model did a thorough analysis of the major and minor losses in the fluidic system and included them in momentum and mass continuity equations as follows:

$$v_2^2 + \frac{P_2}{\rho_2} + \frac{1}{2} K_L \bar{v}^2 = v_1^2 + \frac{P_1}{\rho_1}, \quad (18)$$

where v_1, v_2 and P_1, P_2 are corresponding fluid velocities and pressures at sections 1 and 2, \bar{v} is the mean velocity, and K_L is the minor loss coefficient. Although the acceleration of fluid elements was neglected, the acceleration of solid components, such as piston and load, were incorporated into the model. Active valves made with piezo material were used in this setup; hence, the opening and closing of the valves were controlled by controlled electrical signals. Tan's model is in two forms: although both of them assume the fluid in the pumping chamber to be compressible, the first form, that is, the incompressible viscous flow (IVF) assumed the fluid in the tubing to be incompressible whereas the second form, that is, compressible viscous flow (CVF) considered compressibility in all fluidic parts. In both formulations, the operation of the piezohydraulic pump was broke up into four stages, similar to the approach used earlier by Nasser et al. (2000). For both the IVF and CVF models, the rate of change of fluid pressure in the pumping chamber, P_{ch} , due to displacement x of the driving piezostack was obtained from

$$\dot{P}_{ch} = \beta \frac{A_{ch}}{V - A_{ch}x} \dot{x},$$

where A_{ch} and V are the cross-sectional area and total initial volume of the pumping chamber, respectively. However, for the incompressible model (IVF), there is no change in fluid density when either of the valves are open, that is, $\dot{\rho} = 0$. The CVF model, on the other hand, takes into account the change in fluid density in the pumping chamber due to corresponding flow rates and the corresponding rate of change is given by

$$\dot{\rho}_{ch} = \frac{-V_1 A_p + \dot{x} A_{ch}}{A_{ch}(L_o - x)},$$

where V_1 is the velocity at the entrance/exit of the pipe (positive for outflow, negative for inflow) and A_p is the cross-sectional area of the pipe. This method was shown to be accurate up to ~ 150 Hz pumping frequency, with the CVF model yielding better results than the IVF model as the frequency increased. According to the authors, the reason for this discrepancy is that the CVF model assumed a linear bulk modulus to pressure model, whereas the IVF model assumed an infinite modulus. The authors also carried out a timing study that showed the importance of valve timing to the performance of stack; the different optimal timings for unloaded and loaded systems indicated that the acceleration and inertia of the load and the fluid may influence the performance of the system.

Kim and Wang (2009) developed a time-domain model by using differential equations to account for the changes in pressures within the chamber (P_p) and the actuation cylinder (P_1) as follows:

$$\dot{P}_p = \frac{\beta_e}{(V_c + A_p x_p)} (Q_o - Q_s - A_p \dot{x}_p) \quad (19)$$

$$\dot{P}_1 = \frac{\beta_e}{(V_0 + A_1 x)} (Q_o - Q_1 - Q_p - A_1 \dot{x}), \quad (20)$$

where the respective flow rates were determined by the orifice flow equation:

$$Q = \text{sgn}(\Delta P) C_d A_o \sqrt{\frac{2|\Delta P|}{\rho}}, \quad (21)$$

where C_d is the discharging flow coefficient, A_o is the orifice area, and ΔP is pressure difference between upstream and downstream.

For the reed valve opening (x_R), the reed dynamics was described as a SDOF lumped model, because the nominal operating frequency was lower than the bandwidth of the reed (400 Hz) and would not excite the higher-order modes of the reed valve. The governing equation of the reed opening displacement became

$$m_R \ddot{x}_R + c_R \dot{x}_R + k_R x_R = A_R (P_p - P_1), \quad (22)$$

where $A_R (P_p - P_1)$ was the valve cracking force, and m_R , c_R , k_R , and A_R represent the effective mass, damping constant, effective stiffness, and the orifice area of the reed valve, respectively.

Numerical simulations using these models were not always accurate at high frequencies of operation (> 300 Hz) where the inertia of the transmission fluid become dominant and the material characteristics become highly nonlinear. In addition, all these models were either developed for active valves that control the fluid flow or were operated by electrical signals or assumed the valves to have instantaneous response; hence, they are either completely open or completely closed and their operation was fully determined by

actuating signals rather than the fluid pressure with the system. This is not the case with passive reed valves that would be used in a high-frequency hybrid pump, where the valve openings are strongly dependent on pressure differences across the ports and the dynamics of the metal reeds (Cunningham et al., 1999; Baudille and Biancolini, 2008).

A comprehensive nonlinear time-domain model was developed for the hybrid actuators designed and tested earlier at the University of Maryland (Chaudhuri et al., 2006, 2009). The active material was modeled using linearized quasi-static equations, as the natural frequency of this section was found to be much higher than the frequency range of operation. This model took into account the motion of the pumping piston head mass and the output shaft along with any load mass by considering them as SDOF systems and the respective governing force balance equations. Friction in the output hydraulic cylinder was represented using the Karnopp (1985) model. Compressibility of the fluid in the pumping chamber, the high pressure-driven side, and the manifold tubing were accounted for by incorporating the bulk modulus of the fluid. A coupled lumped parameter approach was used to represent inertia and compliance of the hydraulic fluid in the long manifold passages and the output cylinder. To model the continuously varying openings of the passive reed valves in contrast to on-off type valves, two dynamic variables, r_{out} and r_{in} , were introduced to express the opening of the reed valves as a function of the time-varying pressure difference across the reed ports. This feature allowed simulation of the frequency-dependent behavior of the output piston motion, as noted in experiments (Chaudhuri et al., 2009), and also captured the back flow through the pressure-dependent passive valves, as was reported in earlier studies (Nasser et al., 2001; Rupinsky and Dapino, 2006). Two-dimensional CFD models with fluid-structure coupling were used for the first time to estimate the critical pressures required for opening the reed valves in these hybrid devices, while their dynamic response characteristics were obtained from empirical results. The combined frequency response of the power amplifier and electric/magnetic circuit was also included in the overall system model.

The important variables in different sections of the actuator are shown in Figure 21. The driving force in the actuation system arises from the displacement of the pumping piston, represented by x_p , which results in a change of fluid pressure, P_{ch} , in the pumping chamber. The fluid flows through the manifold tubing into the driving side of the output cylinder, resulting in a change in the pressure P_h . The pressure difference between the high pressure-driven side and the low pressure-driven side, which is connected to a low stiffness accumulator at pressure P_{acc} , provides the driving force to the output shaft and any connected load. The

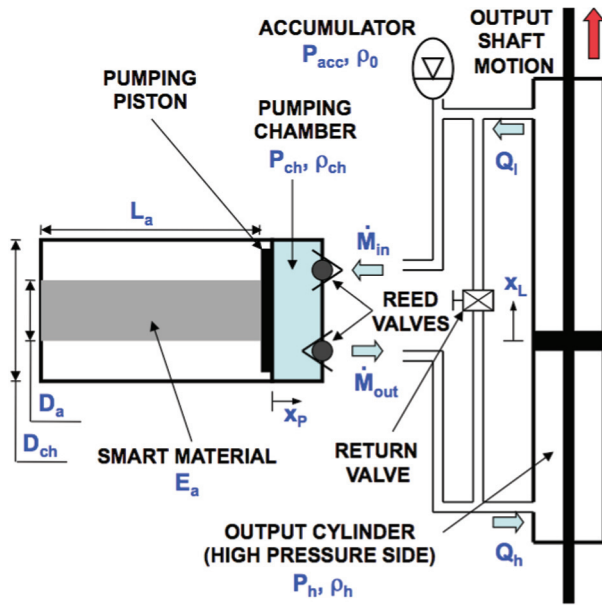


Figure 21. Schematic and important physical variables of hybrid actuator test setup in unidirectional mode of operation (Chaudhuri et al., 2009; Chaudhuri and Wereley, 2010).

mean output velocity of the output shaft is calculated as the slope of a linear fit to the shaft displacement, x_L .

As the continuous motion of the passive reed valves used in the actuator depends only on the pressure differences acting across them, the conditions governing these stages are identified as follows:

1. Discharge: $P_{ch} - P_{th} > 0$
2. Intake: $P_{acc} - P_{ch} > 0$

where P_{ch} is the pressure in the pumping chamber, P_{th} is the entry pressure in the discharge manifold (also the pressure at the discharge reed port exit), and P_{acc} is the pressure in the accumulator. These stages are repeated every pumping cycle and result in a net mass flow rate \dot{M}_{out} out of the pump through the discharge tube and an equivalent mass flow rate \dot{M}_{in} into the pump through the intake tube. The duration of any stage depends on the pressure differential across the valve port and varies with operating conditions.

A comparison of some of the important actuator modeling schemes and their features, along with the model developed in this article, has been summarized in the chart shown in Table 1. Several important aspects of the models have been considered; they are (1) static or dynamic formulation, (2) time or frequency domain, (3) modeling of the active material (nonlinear dynamic model or quasi-static linearized model), (4) SDOF representation of pumping piston and output load, (5) fluid

Table 1. Survey of models.

Model Reference	Static (S)/dynamic (D)	Frequency (F)/time (T) domain	Active material (static/dynamic)	SDOF representation	Fluid compressibility	Fluid inertia	Viscous losses	Valve dynamics	CFD	Friction model
Chaudhuri et al. (2009)	D	T	●	●	●	●	●	●	●	●
Kim and Wang (2009)	D	T	●	●	●	●	●	●	●	●
Tan et al. (2005)	D	T	●	●	●	●	●	●	●	●
Regelbrugge et al. (2003)	D	T	●	●	●	●	●	●	●	●
Oates and Lynch (2001)	D	T	●	●	●	●	●	●	●	●
Sirohi et al. (2005)	D	F	●	●	●	●	●	●	●	●
Ullmann and Fono (2002)	D	F	●	●	●	●	●	●	●	●
Nasser et al. (2001)	D	T	●	●	●	●	●	●	●	●
Cadou and Zhang (2003)	S	T	●	●	●	●	●	●	●	●
Sirohi and Chopra (2003)	S	T	●	●	●	●	●	●	●	●
Tang et al. (1997)	D	F	●	●	●	●	●	●	●	●

compressibility, (6) fluid inertia, (7) flow losses (viscous and/or minor), (8) use of CFD, (9) dynamics of the rectifying valves, and (10) friction in output hydraulic cylinder. A full (or half) circle means that the corresponding feature was included completely (or partly) in the model, whereas an empty box refers to absence of that property in the formulation. As seen from the chart, a majority of the models incorporated frequency-dependent dynamic effects; the models by Sirohi and Chopra (2003) and Cadou and Zhang (2003) were static in nature and hence used a time-domain approach. Almost all the models used the quasi-static linearized equations governing the behavior of the active material; the model by Tang et al. (1997) took a more exhaustive look at the dynamics of a stacked actuator (as shown by the complete circle). Both the pumping piston and the output load were represented by mass-spring-damper equivalents (Nasser et al., 2001; Oates and Lynch, 2001; Ullmann et al., 2001; Ullmann and Fono, 2002; Regelbrugge et al., 2003; Sirohi et al., 2005); Tan et al. (2005) modeled only the output load using this approach. Fluid compressibility was included in most cases; however, Sirohi and Chopra (2003) and Cadou and Zhang (2003) assumed the fluid to be compliant only in the pumping chamber and incompressible in the rest of the manifold. Fluid inertia was also included in some of the models; however, the coupling (shown by the dashed boxes encircling the two corresponding entries in the chart) between the inertia and compressibility was previously considered only by Nasser et al. (2001) and Sirohi et al. (2005).

Mechanical Components

Pump piston and pumping chamber. As the movement of the active material provides energy to the whole system, the pumping action of the active rod/stack is modeled first. Denoting the fluid pressure inside the pumping chamber as P_{ch} , the equation of motion of the pumping piston (Figure 22(a)), by considering it as a SDOF system, is as follows:

$$\left(M_P + \frac{M_A}{3}\right)\ddot{x}_P + C_P\dot{x}_P + (K_a + K_d + K_s)x_P = K_a d_a B L_a - P_{ch} A_{ch}, \quad K_a = \frac{E_a A_a}{L_a}. \quad (23)$$

The stiffness of the metal diaphragm, K_d , was calculated from empirical relations (Blevins, 1979), whereas the disk spring stiffness, K_s , was obtained from manufacturer supplied data. The mass of the actuator rod, M_A , was also included in the effective mass being accelerated, as the rod can be visualized as a spring with nonzero mass (Galloni and Kohen, 1979; Wallach et al., 1988; Santos et al., 2006).

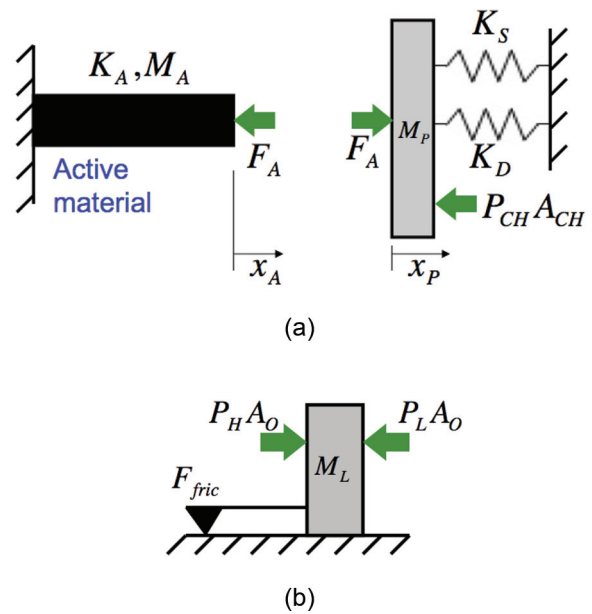


Figure 22. Free-body diagrams for the pumping piston and output cylinder shaft: (a) pumping piston and (b) output cylinder shaft.

Although the strain induced in the active material is a nonlinear phenomenon and can also vary with prestress, the piezoelectric/piezomagnetic coefficient, d_a , of the material is assumed to be constant to obtain a simpler macroscopic view of the physical phenomenon without going into the details of microscopic material properties that govern the transduction behavior. For the same reason, any variation in Young’s modulus, E_a , of the active material as a function of prestress, usually noted in magnetostrictive materials such as Terfenol-D and called the ΔE effect (Clark et al., 1983; Dapino et al., 2000; Kellogg and Flatau, 2001; Kellogg and Flatau, 2004), are neglected.

Output cylinder. The equation of motion of the output cylinder shaft was obtained from force equilibrium between the two sides of the output cylinder piston as follows:

$$M_L \ddot{x}_L + c_L \dot{x}_L = (P_h - P_l) A_o - F_{fric} - F_{ext}, \quad (24)$$

where F_{ext} includes any external forces that might be acting on the output cylinder, for example, $F_{ext} = m_L g$ for a mass hung from the cylinder shaft, and F_{fric} the frictional force acting on the output piston, arising mainly from seals in the assembly that make contact between the piston shaft and the walls of the hydraulic cylinder (Lai and Kay, 1993; Parker Hannifin Corporation, 2001). F_f was based on the symmetric Karnopp model (Karnopp, 1985; Armstrong-Hélouvy et al., 1994; de Wit et al., 1995; Olsson et al., 1998) and depends on the applied force, F , and instantaneous velocity, v , as follows:

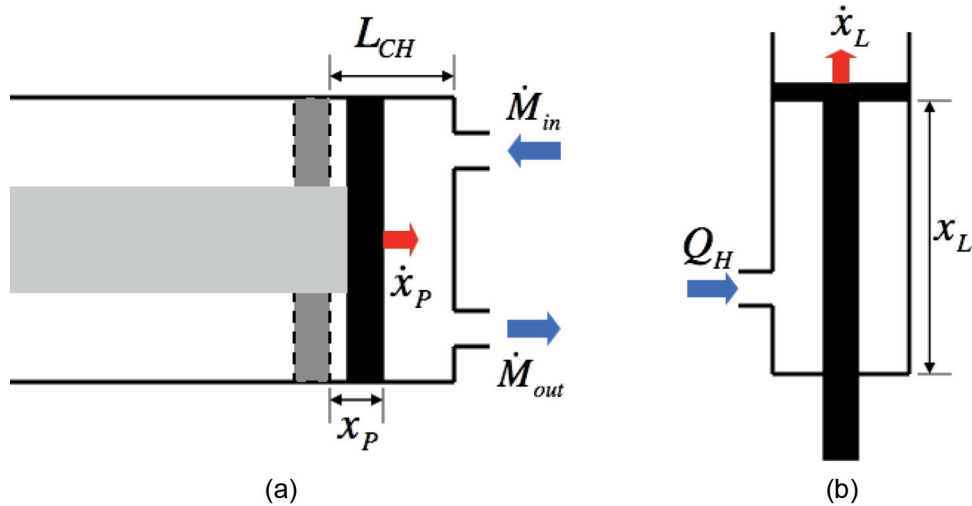


Figure 23. Volume changes and flow rates in compressible sections: (a) pumping piston and (b) output cylinder (high pressure-driven side).

$$F_f = \begin{cases} \text{sgn}(v)F_d & , |v| > v_{min} \\ \text{sgn}(F)\max(F, F_s) & , |v| \leq v_{min} \end{cases} \quad (25)$$

where $F = (P_h - P_{acc})A_o - F_{ext}$ is the total force acting on the output piston. F_s and F_d are the static and dynamic friction in the output hydraulic cylinder, respectively.

Fluid Compressibility

Pumping chamber and output cylinder (high-pressure side). The fluid density in the pumping chamber (Figure 23(a)) is (Regelbrugge et al., 2003; Tan et al., 2005; Chaudhuri et al., 2009; Kim and Wang, 2009)

$$\dot{\rho}_{ch} = \frac{\rho_{ch}A_p\dot{x}_p - \dot{M}_{out} + \dot{M}_{in}}{A_p(L_{ch} - x_p)} \quad (26)$$

and the corresponding rate of pressure change inside the chamber is

$$\dot{P}_{ch} = \beta \frac{\dot{\rho}_{ch}}{\rho_{ch}} = \beta \frac{(\rho_{ch}A_p\dot{x}_p - \dot{M}_{out} + \dot{M}_{in})}{\rho_{ch}A_p(L_{ch} - x_p)} \quad (27)$$

Similarly, in the driving side of output cylinder (Figure 23(b)), the density of the fluid is governed by the flow rate into the cylinder and the motion of the piston (Richer and Hurmuzlu, 2000), which are included in the following equation:

$$\dot{\rho}_h = \frac{\rho_h Q_h - \rho_h A_o \dot{x}_L}{A_o x_L} \quad (28)$$

where $A_o = \pi(D_o^2 - D_i^2)/4$, and the corresponding change in pressure is given by

$$\dot{P}_h = \beta \frac{\dot{\rho}_h}{\rho_h} = \beta \frac{(Q_h - A_o \dot{x}_L)}{A_o x_L} \quad (29)$$

Accumulator. Due to the presence of a low stiffness accumulator on the low-pressure driven side of the pump, it was assumed that the motion of fluid in this section results only in deformation of the accumulator diaphragm, and consequently, fluid compressibility effects are negligible in this section (Sirohi et al., 2005). Applying mass continuity for this section of the actuator,

$$\rho_0 A_{acc} \dot{x}_{acc} = \rho_0 Q_l - \dot{M}_{in} \quad (30)$$

and the resulting accumulator pressure variation is

$$\dot{P}_{acc} = \frac{K_{acc} \dot{x}_{acc}}{A_{acc}} = \frac{K_{acc}(\rho_0 Q_l - \dot{M}_{in})}{\rho_0 A_{acc}^2} \quad (31)$$

Fluid Inertia

Flow passages. Model of transient fluid flow through the high pressure-driven side manifold and the low-pressure-driven side of the output cylinder took into account the inertia of the fluid mass and the viscous losses. For flow in 1D in uniform cross-sectional passage, the equation of motion and the continuity equation of fluid mechanics can be used to derive the governing partial differential equations (PDEs), commonly referred to as the *waterhammer equations* and analogous to *transmission line* models in electrical engineering (Wylie and Streeter, 1983; Ghidaoui, 2004). To get ordinary differential equations for simulation in the time-domain model, the transmission line analogy is applied to the manifold tubing (Figure 24(a)) and low-pressure-driven side of output cylinder (Figure 24(b)) by breaking up each passage into equal length sections along the longitudinal axis and assuming that the volume flow rate and fluid density in any section are constant; rate equations for the volume flow rate

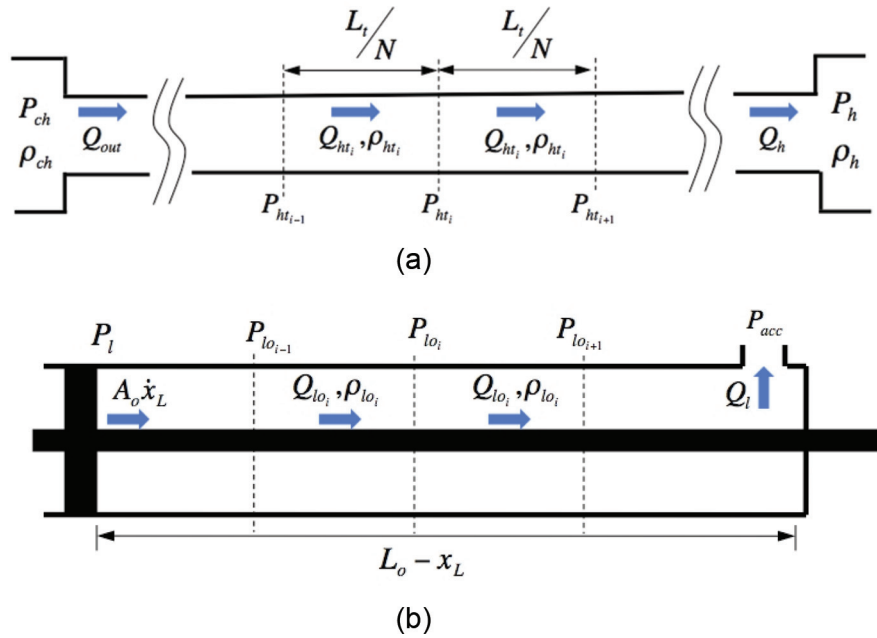


Figure 24. Lumped models for transient fluid flow: (a) manifold tubing passage and (b) low-pressure side of output cylinder.

(Equation (32)) and pressure (Equation (34)) though each section were then formulated for each of the *lumps* (Doebelin, 1980; Watton, 1989; Manring, 2005).

For the manifold tubing, the pressure drop across any section can be accounted for the effects of fluid inertia and viscous losses as follows (Doebelin, 1980; Nasser et al., 2001):

$$P_{ht_i} - P_{ht_{i+1}} = \frac{(L_t/N_t)}{A_t} \rho_{ht_i} \dot{Q}_{ht_i} + R_t \left(\frac{L_t}{N_t} \right) \rho_{ht_i} Q_{ht_i}, \quad (32)$$

where N_t is the total number of sections for the tubing and R_t is the viscous resistance to fluid flow in the circular passage per unit length based on the quasi-static friction model used in unsteady pipe flows (Adamkowski, 2003, 2006). From the measured velocities, the maximum Reynolds number for flow through the tubing was found to be 150. Hence, the viscous fluid resistance can be calculated from the Hagen–Poiseuille solution for laminar flow through a circular tube (White, 1979), that is,

$$\Delta P_{laminar} = \frac{128\nu}{\pi D^4} L \rho Q \Rightarrow R = \frac{8\pi\nu}{A^2}. \quad (33)$$

The change in pressure in section i is dependent on the fluid flow rates in/out of the section as follows:

$$\dot{P}_{ht_i} = \beta \frac{(Q_{ht_i} - Q_{ht_{i+1}})}{A_t(L_t/N_t)}. \quad (34)$$

A similar approach is applied to the output cylinder too, where the length of the driven side, $L_o - x_L$, is broken up into N_o sections, each having a uniform

circular cross section with area A_o . Differential equations for the pressure P_{lo_i} and Q_{lo_i} can then be written.

The known boundary values for the manifold tubing are

$$Q_{ht_1} = Q_{out}, \quad P_{ht_{N_t}} = P_h$$

whereas the calculated boundary variables are

$$P_{th} = P_{ht_0}, \quad Q_h = Q_{ht_{N_t}}$$

For the fluid in the driven side of the output cylinder, the known boundary values are

$$Q_{lo_1} = A_o \dot{x}_L, \quad P_{lo_{N_o}} = P_{acc}$$

whereas the calculated variables are

$$P_l = P_{lo_1}, \quad Q_l = Q_{lo_{N_o}}.$$

Due to the presence of a highly compliant accumulator in the intake side, the fluid in this part of the manifold can be assumed to be incompressible (Sirohi et al., 2005; Tan et al., 2005; Chaudhuri et al., 2006; Chaudhuri and Wereley, 2007) and we can model the entire passage as a single block of fluid being accelerated during every cycle when the intake reed valve is open. If P_{tl} is the pressure at the entry of the intake reed port, then the intake volume flow rate Q_{in} is governed by

$$P_{acc} - P_{tl} = \frac{L_t}{A_t} \ddot{M}_{in} + R_t L_t \dot{M}_{in} + \frac{1}{2} \rho_0 K_{L_t} \left(\frac{\dot{M}_{in}}{\rho_0 A_t} \right)^2, \quad (35)$$

where K_{L_i} is the loss factor associated with minor losses in the intake tubing.

MRFs. To model the annular flow (Yoo and Wereley, 2005), the above approach is simplified (John et al., 2008). For very low volume flow rates, we can assume that the fluid volume flowing through all sections is the same, that is, $Q_i = Q \forall i = 1, 2, \dots, N$. Using this, the pressure drops over the entire length of the MR valve can be summed to get an expression for the overall loss in pressure ΔP_{MR} as a function of the volume flow rate Q as follows:

$$\begin{aligned} \Delta P_{MR} &= \sum_{i=1}^N (P_i - P_{i+1}) \\ &= \frac{L_{MR}}{A_{MR}} \left(\frac{1}{N} \sum_{i=1}^N \rho \right) \dot{Q} + R_v L_{MR} Q. \end{aligned} \quad (36)$$

Furthermore, if the fluid density varies linearly along the length of the valve, then the summation term in Equation (36) can be replaced by the arithmetic mean of the fluid densities at either end of the valve, that is,

$$\Delta P_{MR} = \frac{L_{MR}}{A_{MR}} \frac{(\rho_1 + \rho_N)}{2} \dot{Q} + R_v L_{MR} Q. \quad (37)$$

Rectification Valves and Ports. Passive reed valves perform the function of flow rectification, wherein the bidirectional motion of the active stack is converted to unidirectional flow of fluid by responding to the pressure difference across the respective valve ports. The behavior of a reed valve under varying flow rates depends strongly on the geometrical parameters of the assembly (Naik et al., 2002; Tarnopolsky et al., 2002). Everything else remaining the same, the thickness of the reed (and hence, its stiffness) governs the force required to fully open the valve (Baudille and Biancolini, 2008; Baudille et al., 2009). Unlike on-off valves, a reed valve allows a continuously varying flow through it depending on the amount of deflection of the reed and the geometry of the flow path (Chaudhuri et al., 2006, 2009). As the behavior of the reed valve in our system is analogous to a cantilever beam fixed at one end, the dynamics of the reed can be represented by a second-order system characterized by a natural frequency, ω_n , and damping coefficient, ζ (Junwu et al., 2005). To implement this behavior of the reed valve, the parameter, r_c , which denotes the commanded amount of reed deflection depending on the pressure difference, ΔP , across the reed port is defined as follows (Chaudhuri and Wereley, 2007, 2010; John et al., 2008; Chaudhuri et al., 2009):

$$r_c = \begin{cases} 1 & \text{if } \Delta P > P_{open} \\ \Delta P / P_{open} & \text{if } |\Delta P| \leq P_{open} \\ -1 & \text{if } \Delta P < -P_{open} \end{cases}, \quad (38)$$

where P_{open} is the pressure difference for the reed valve to fully open. The actual valve opening, r , was then related to the input or commanded reed deflection using the following second-order transfer function

$$\frac{r(s)}{r_c(s)} = \frac{1}{1 + \frac{2\zeta}{\omega_n} s + \frac{s^2}{\omega_n^2}} \quad (39)$$

and led to two state equations (r and \dot{r}) for each valve.

For the discharge reed valve, the opening r_{out} was determined by the pressure difference $\Delta P_{out} = P_{ch} - P_{th}$ across the valve, whereas the intake valve opening r_{in} was controlled by the pressure difference $\Delta P_{in} = P_{acc} - P_{ch}$. The parameters, r_{in} and r_{out} , were then used to derive equations for the volume flow rate in and out of the pumping chamber based only on the pressure differences across the reed valve ports. The values of P_{open} and ω_n are strongly dependent on the geometry of the reed valve; an estimate of ω_n was obtained from empirical formulae (Blevins, 1979, 1990), whereas the value of P_{open} was obtained from the results of a fluid-structure interaction study between the reed and the hydraulic oil (discussed in a later section).

The pressure drop incurred in the reed valve ports due to only minor losses can now be expressed in terms of the reed valve openings, r_{out} and r_{in} , and the corresponding fluid velocities as follows:

$$(\Delta P_{out})_{minor} = \frac{1}{2} \rho_{ch} \left(\frac{K_{Lvalue}}{r_{out}} \right) \left(\frac{\dot{M}_{out}}{\rho_{ch} A_{port}} \right)^2 \quad (40)$$

$$(\Delta P_{in})_{minor} = \frac{1}{2} \rho_0 \left(\frac{K_{Lvalue}}{r_{in}} \right) \left(\frac{\dot{M}_{in}}{\rho_0 A_{port}} \right)^2 \quad (41)$$

where K_{Lvalue} is the minor loss coefficient for a fully open reed valve. This definition of the loss coefficient from the reed valve opening is similar to the approach used by Sirohi and Chopra (2001).

The behavior of three different thicknesses of reed valves being forced by a sinusoidally varying pressure at the input face was carried out by Chaudhuri et al. (2009) using CFD; 2D geometry was considered along with an incompressible fluid. Initially, increase in pressure difference across the reed port causes an increase in the volume flow rate, proportional to the mean velocity, through the port. However, due to limited space within the reed port, the flow became highly constricted when the reed valve opened fully, resulting in a decrease in flow rate beyond a certain value of pressure. In other words, there is a particular value of pressure at which the valve can be assumed to be completely open and the viscous losses are least; this value of pressure is used as representative of the parameter P_{open} in the dynamic simulation model (Equation (38)).

This comparative study of reed valve behavior also showed the dependence on reed thickness and reed port geometry. While a thinner reed requires lower pressure

difference to open completely, the maximum volume flow rate through it is also more limited than a thicker reed. Hence, the choice for reed thickness has to be made by comparing the flow rate requirements with the allowable pressure losses in the reed valve. The geometry of the port can also be modified to improve the performance of the valve; filleting the sharp edges of the reed port will help in improving flow rate (John et al., 2006).

The complete governing equations for the pulsating flow through the reed ports that take into account the fluid inertia, viscous fluid resistance, and minor losses inside the ports, are given by

$$(\Delta P_{out})_{total} = P_{ch} - P_{th} = \frac{L_{port}}{A_{port}} \rho_{ch} \ddot{M}_{out} + R_{port} L_{port} \rho_{ch} \dot{M}_{out} + (\Delta P_{out})_{minor} \quad (42)$$

$$(\Delta P_{in})_{total} = P_{tl} - P_{ch} = \frac{L_{port}}{A_{port}} \rho_0 \ddot{M}_{in} + R_{port} L_{port} \rho_0 \dot{M}_{in} + (\Delta P_{in})_{minor}, \quad (43)$$

where P_{tl} is the manifold fluid pressure at the intake reed port entry. By summing up the pressure drops in Equations (35) and (43), a single governing ODE for the intake mass flow rate, \dot{M}_{in} , as a function of the pressures at its two ends and the intake reed valve opening is obtained.

Simulation Results. Equations (23), (24), (27), (29), (31), (35), (39), and (42), along with $2(N_i + N_o)$ equations from Equations (32) and (34) for the manifold tubing, can be written in state-space form, where the states are given by

$$x = [x_P \quad \dot{x}_P \quad x_L \quad \dot{x}_L \quad P_{ch} \quad P_h \quad P_{acc} \quad \dot{M}_{out} \quad \dot{M}_{in} \quad r_{out} \quad \dot{r}_{out} \quad r_{in} \quad \dot{r}_{in} \quad P_{ht1} \dots P_{htN_i} \quad Q_{ht1} \dots Q_{htN_i} \quad P_{lo1} \dots P_{loN_o} \quad Q_{lo1} \dots Q_{loN_o}]$$

and solved in time-stepped manner using a fourth-order Runge-Kutta numerical scheme. Some of the main material properties and geometric parameters used for simulation are given in Table 2.

The frequency at which peak no-load performance occurs mainly depends on two properties, inertia and stiffness, of the actuation system. In general, the inertia of the system consists of the inertia of the pump piston, the output cylinder and the fluid being accelerated through the valves and manifold. When viewed as separate SDOF systems, the masses of the pump piston and the output cylinder (with no external load) are very small, whereas the corresponding stiffnesses and driving forces are very large; hence, these systems have a high natural frequency and do not impose any limitations in our frequency range of operation. However, the fluid in the manifold has a stronger inertia effect due to the

Table 2. Simulation parameters for smart actuators.

	Magnetostrictive	Electrostrictive
β	70 MPa (10 ksi)	550 MPa (80 ksi)
ρ_0	860 kg/m ³	871 kg/m ³
E_a	30 GPa	12 GPa
L_{ch}	0.51 mm	2.54 mm
D_{ch}	38.1 mm (1.5 inch)	31.75 mm (1.25 inch)
L_0	50.8 mm (2.0 inch)	50.8 mm (2.0 inch)
A_0	253.4 mm ²	128.9 mm ²
m_p	200 g	75 g

long travel distance and the small cross-sectional area available in the compact manifold (Figures 25–27).

The location of the actuator peak output is very sensitive to value of fluid bulk modulus (Chaudhuri, 2008), which should ideally be very high to transfer all the energy from the active material to the load. The presence of entrained air in the hydraulic oil increases the fluid compressibility and drastically reduces the bulk modulus (Merritt, 1967; Oates and Lynch, 2001; Niezrecki et al., 2004; Sneed et al., 2006; Kim and Wang, 2009) as seen from the data sheet for hydraulic oil in Figure 28. In practice, entrained air is removed from the oil by using a vacuum pump after filling the actuator manifold and then pressurized to minimize the effects of any remaining entrained air. The value of bulk modulus used in the numerical simulations is much lower than the manufacturer specified value. Increasing the value of bulk modulus stiffens the fluid, thus moving the resonant peak to a higher frequency. In addition, a stiffer fluid causes lower pressure losses, because less force is lost in compressing the fluid volume in the manifold before it begins to flow (Figure 28). The disadvantage of having a higher bulk modulus is that the stiffness of the pumping chamber, K_{ch} , which is derived as (Sirohi and Chopra, 2003)

$$K_{ch} = \beta \frac{A_p}{L_{ch}} \quad (44)$$

increases linearly with the value of bulk modulus and results in lower induced strain from the actuator rod; as a consequence, the mass flow rate of hydraulic fluid from the pumping chamber reduces (Giurgiutiu et al., 1997). Hence, the design of the actuator for particular specifications involves a trade-off between the desired maximum pressure (corresponding to blocked force) and maximum flow rate (corresponding to no-load output velocity). For a given working fluid, β is fixed, and A_p may be constrained by flow rate requirements; in such a case, the only parameter which the designer is free to choose is the pumping chamber height, L_{ch} .

A noticeable feature is the oscillatory behavior seen in the displacement data; for the magnetostrictive-based actuator, the measured displacement at lower

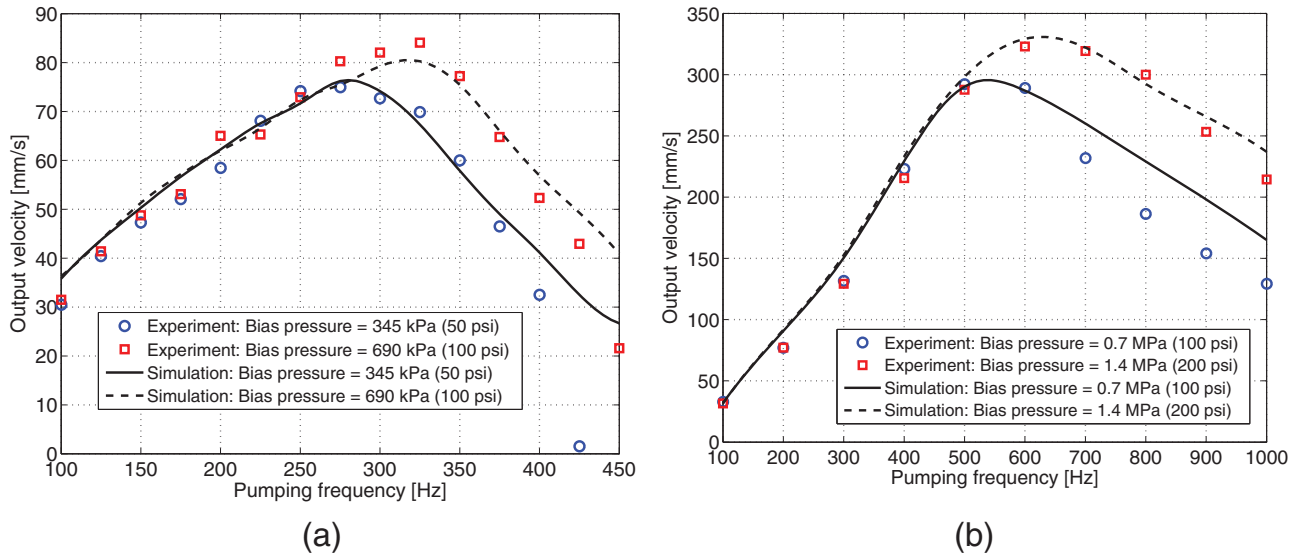


Figure 25. Comparison of measured output velocity with simulation results at different pumping frequencies and bias pressures: (a) Terfenol-D-based actuator and (b) PMN-PT-based actuator.

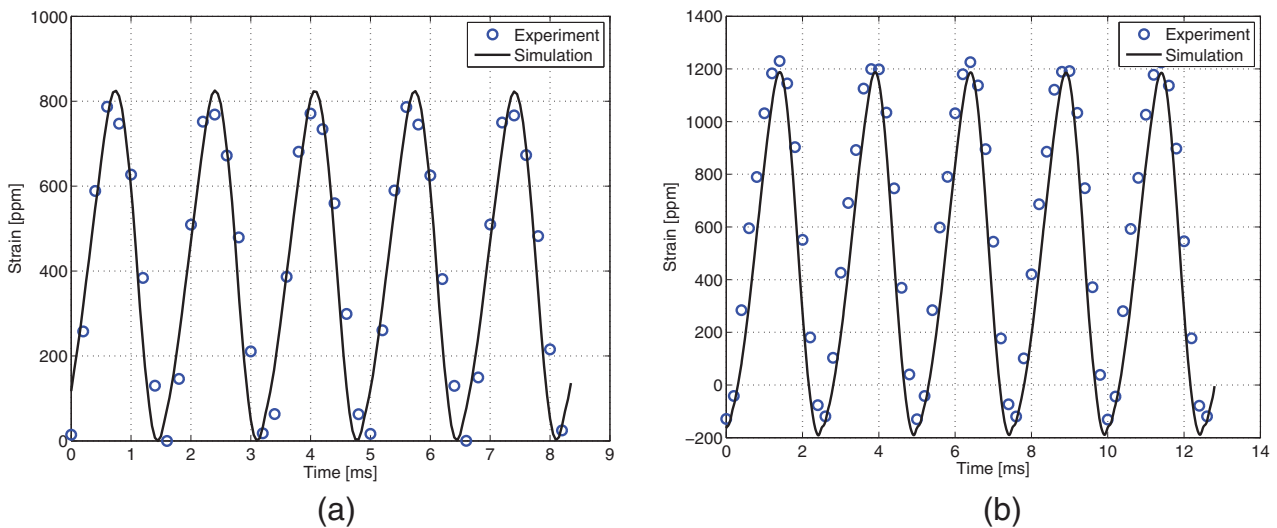


Figure 26. Comparison of induced strain in PMN-PT stack with simulation results under different driving conditions: (a) induced strain in PMN stack at 300 V, 600 Hz and (b) induced strain in PMN stack at 400 V, 400 Hz.

frequencies (Figure 29(a)) resembles a lightly damped system, whereas the motion at higher frequencies did not show any overshoot (Figure 29(b)). The comprehensive model does a good job at capturing this variation in damping, as well as tracking the initial and final positions of the output piston in each pumping cycle. Numerical simulations show that this behavior was strongly dependent on the dynamics of the reed valves and the stiction behavior of the output piston.

Figure 30 shows a comparison between models developed earlier that neglected unsteady effects and the comprehensive model (Chaudhuri et al., 2009; Chaudhuri and Wereley, 2010). The two other models considered are as follows:

1. *Incompressible, inviscid fluid*: The simplest model assumes an incompressible, inviscid fluid with no inertia. By combining Equations (1) and (2), we get

$$v_L = f \times (\varepsilon L_a) \times (A_{ch}/A_o), \quad (45)$$

which shows that $v_L \propto f$ (Sirohi and Chopra, 2003). These calculations overestimate the output velocity to a large extent because they did not include any pressure losses in the fluidic subsystem and assumed that the maximum possible strain was induced in the active material. Hence, this method serves as a good starting point for the selection of material and

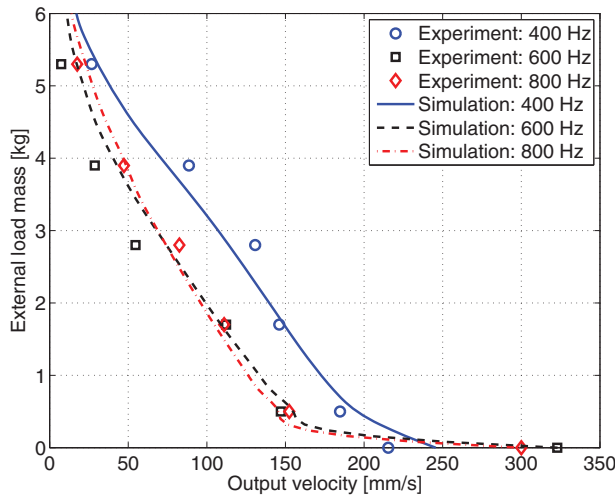


Figure 27. Comparison of experimental and simulation results under loaded conditions (Force–Velocity diagrams).

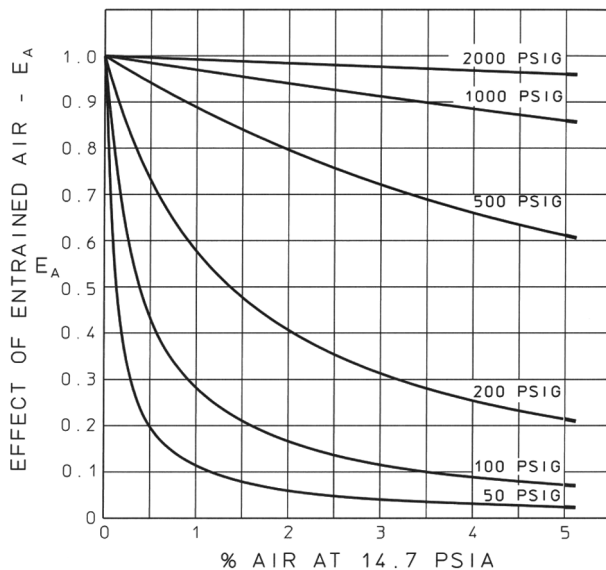


Figure 28. Effect of entrained air on the bulk modulus of a fluid (The Lee Company, 2006).

actuator design, but it cannot be used for accurate predictions.

2. *Compressible fluid, no inertia:* Using the approach developed by Tan et al. (2005), the results for a model that included viscosity and area changes but neglected flow unsteadiness were computed. The low-frequency results were well matched, but the simpler model deviated from test results at higher pumping frequencies and also failed to capture the sharp roll-off observed beyond the peak output frequency. These results were similar to those calculated previously by the authors for a magnetostrictive-based actuator (Chaudhuri, 2008; Chaudhuri et al., 2009).

Assessment Of Current Technology And Future Work

The development of smart material–based compact electrohydraulic actuators has reached a considerable amount of maturity, as is evident by the recent 2009 Smart Structures Product Implementation Award presented to Kinetic Ceramics Inc. by SPIE. Power output and volumetric flow rates achievable from these compact devices have also increased over the last decade. This article presents an overview of smart material–based compact electrohydraulic pumps and actuators that have been investigated in recent years. The development and performance of some of these complex devices has been outlined, and the efforts into modeling and simulation of the complex and coupled phenomena in these actuators have also been reviewed.

Limitations in Current Designs

1. *Actuator mechanical stiffness:* Although currently available smart materials such as PZT-5H and Terfenol-D have high mechanical stiffness in their monolithic form, their configuration in practical use lowers the effective mechanical stiffness. For example, stacking thin layers of piezoelectric and electrostrictive materials with electrode material packed in between to build an actuator drastically lowers the effective modulus. In case of magnetostrictive materials, the actuator rods have to be laminated to minimize the adverse effects of eddy currents at high frequencies. The only solution at present is to use actuators with higher cross-sectional area, thus increasing the size of the device and reducing the output power-to-weight ratio.
2. *Fluid inertia and compressibility:* As fluid pumping frequencies are increased, the effect of inertia of the fluid volume that has to be accelerated each cycle increases quadratically. This leads to more and more energy being used to start or stop fluid motion, rather than improving flow rate. The problem worsens when the fluid is highly compressible, which wastes energy required to compress (and then move) the fluid mass during the compression and discharge cycles (Figure 3). Ways to improve efficiency include minimizing the volume of entrained air and pressurizing the fluidic subsystem.
3. *Bandwidth of driving circuit:* This effect is dominant in the case of magnetoactive materials that have to be actuated using a magnetizing coil, where the presence of an inductive coil limits the frequency bandwidth of the driving electrical circuit (Chaudhuri et al., 2009). Compensating electronics may be required for high-frequency operation.

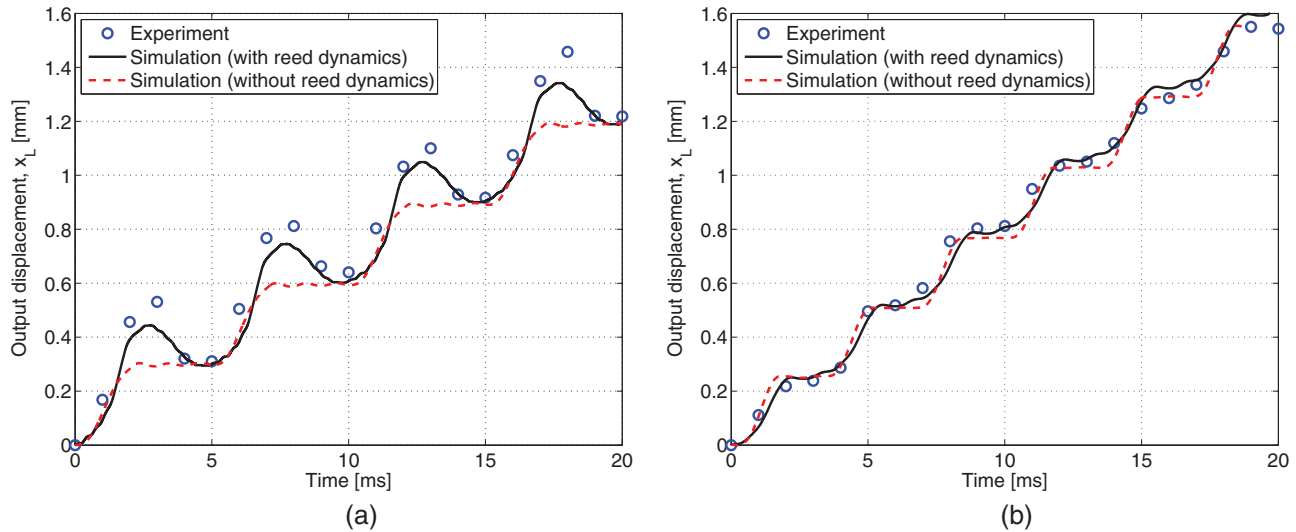


Figure 29. Comparison of measured output piston displacement with simulation results (with and without reed valve dynamics): (a) pumping frequency = 200 Hz and (b) pumping frequency = 300 Hz.

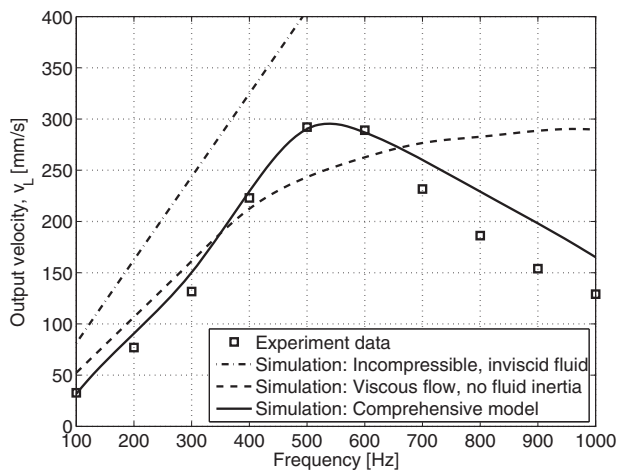


Figure 30. Simulation results with different models.

4. *Flow rectification using valves* (Tieck et al., 2005): On the basis of earlier studies, it is clear that the combination of a smart stack/rod actuator with fast response valves is crucial to the development of a high-frequency, high power density, and intrinsically reliable piezoelectric pump (Lee et al., 2004). Studies of active valve-based systems have shown that the valve timing is also critical to the performance of the system (Tan et al., 2005).

Improvements in Analytical Modeling

Modeling and simulation of smart material-driven electrohydraulic actuators have progressively improved over the last decade. These formulations take a macroscopic look at the operation of the hybrid pump and,

in some cases, combine it with the dynamics of the different sections using either a frequency-domain or a time-domain approach. This allows the engineer to get an accurate measure of a particular design without actually building and testing a prototype using easily obtainable property values and even allows for optimizing the design. Using a time-domain formulation, the model can more accurately include nonlinear effects such as logarithmic dependence of fluid density on bulk modulus, friction in output cylinder, and quadratically varying pressure losses in the fluid passages. Although the present models perform well at calculating the performance of the hybrid actuator over a large frequency range and varying loading conditions, certain issues can be considered to increase modeling accuracy:

1. The induced strain in the active material varies nonlinearly in reality (Wan et al., 2003; Sirohi et al., 2005), especially when the material is actuated over its entire range. A complete dynamic model of the active material that accurately reflects the behavior with stress dependence can be used for more accuracy for magnetostrictive materials (Engdahl, 1999). The linearized model is deemed sufficient in most models because it is simpler to implement and reduces the computational loads that usually accompany the energy-based material models (Hom and Shankar, 1997, 1999; Smith, 1997; Dapino et al., 2000).
2. An accurate estimation of the fluid bulk modulus (β) is extremely important. Some further modeling refinements can be made if fluid pressure measurements are made at additional locations (e.g., pumping chamber, discharge port, driving side of output cylinder, intake manifold)

during pump operation and compared with simulation results. However, it should be kept in mind that any pressure tap will act as a source of compliance within the fluidic system and can reduce the effective bulk modulus.

- There have been some studies of reed valve motion in smart electrohydrostatic actuators (Walters, 2008). A complete 3D coupled simulation of the reed valve port can be used to obtain accurate values of the loss coefficients therein. However, in addition to being computationally intensive, this calculation would have to be repeated for any small changes in port geometry or fluid properties (John et al., 2009).

References

- Adamkowski A (2003) "Analysis of Transient Flow in Pipes with Expanding or Contracting Sections," *Journal of Fluids Engineering—Transactions of the ASME*, 125(4): 716–722. DOI: 10.1115/1.1593703.
- Adamkowski A and Lewandowski M (2006) "Experimental Examination of Unsteady Friction Models for Transient Pipe Flow Simulation," *Journal of Fluids Engineering—Transactions of the ASME*, 128(6): 1351–1363. DOI: 10.1115/1.2354521.
- Anderson E and Garg DP (2002) "Active Vibration Control in Rotorcraft Systems Using Smart Actuators," In: *43rd AIAA/ASME/ASCE/AHS/ASC Structures, Structural Dynamics, and Materials Conference*, AIAA-2002-1434 (11 pages), Denver, CO.
- Anderson E, Bales GL and White EV (2003) "Application of Smart Material—Hydraulic Actuators," In: *Proceedings of the SPIE: Industrial and Commercial Applications of Smart Structures Technologies*, Vol. 5054, SPIE, San Diego, CA, pp. 73–84. DOI: 10.1117/12.483896.
- Anderson E, Lindler J and Regelbrugge M (2002) "Smart Material Actuator with Long Stroke and High Power Output," In: *43rd AIAA/ASME/ASCE/AHS/ASC Structures, Structural Dynamics, and Materials Conference*, AIAA-2002-1354 (9 pages), AIAA, Denver, CO.
- Armstrong-Hélouvy B, Dupont P and de Wit CC (1994) "A Survey of Models, Analysis Tools and Compensation Methods for the Control of Machines with Friction," *Automatica*, 30(7): 1083–1138. DOI: 10.1016/0005-1098(94)90209-7.
- Barsoum RGS (1997) "Active Materials and Adaptive Structures," *Smart Materials and Structures*, 6(1): 117–122. DOI: 10.1088/0964-1726/6/1/014.
- Baudille R and Biancolini ME (2008) "A General Approach for Studying the Motion of a Cantilever Beam Interacting with a 2D Fluid Flow," *Interaction and Multiscale Mechanics*, 1(4).
- Baudille R, Biancolini ME and Mottola E (2009) "Non-Linear Models of Reed Valve Dynamics," *International Journal of Vehicle Systems Modelling and Testing*, 4(3): 150–184. DOI: 10.1504/IJVSMT.2009.029387.
- Beckman JB and Blickstein MJ (1984) "Apparatus and Method for Piezoelectric Pump," *US Patent* 4,449,893.
- Beckman JB and Blickstein MJ (1985) "Piezoelectric Pump with Internal Load Sensor," *US Patent* 4,519,751.
- Bishop RP, Face BR, Face SA, Clark SE and Rose NS (2000) "Piezoelectrically Actuated Piston Pump," *US Patent* 6,071,088.
- Blevins RD (1979) *Formulas for Natural Frequency and Mode Shape*, Van Nostrand Reinhold Company, New York.
- Blevins RD (1990) *Flow Induced Vibration*, 2nd edn. New York: Van Nostrand Reinhold Company.
- Bouchilloux P, Claeysen F and Le Letty R (2004) "Amplified Piezoelectric Actuators: From Aerospace to Underwater Applications," In: *Proceedings of the SPIE Symposium on Smart Structures and Materials*, Vol. 5388, SPIE, San Diego, CA, pp. 143–154. DOI: 10.1117/12.540781.
- Bridger K, Cooke AV, Crowne FJ, Lutian JJ, Sewell JM and Small GL III. (2004) "Compact Hybrid Actuator," *US Patent* 6,751,954.
- Bridger K, Sewell JM, Cooke AV, Lutian JL, Kohlhafer D, Small GE and Kuhn PM (2004) "High Pressure Magnetostrictive Pump Development: A Comparison of Prototype and Modeled Performance," In: *Proceedings of the SPIE*, Vol. 5388, SPIE, San Diego, CA, pp. 246–257. DOI: 10.1117/12.548481.
- Butler JL (1988) *Application Manual for the Design of ETREMA Terfenol-D Magnetostrictive Transducers*, Etrema Products, Inc., Ames, IA.
- Cadou C and Zhang B (2003) "Performance Modeling of a Piezo-Hydraulic Actuator," *Journal of Intelligent Material Systems and Structures*, 14(3): 149–160. DOI:10.1177/1045389X03014003003.
- Calkins FT, Dapino MJ and Flatau AB (1997) "Effect of Prestress on the Dynamic Performance of a Terfenol-D Transducer," In: *Proceedings of the SPIE*, Vol. 3041, SPIE, San Diego, CA, pp. 293–304. DOI:10.1117/12.275654.
- Carlson JD and Jolly MR (2000) "MR Fluid, Foam and Elastomer Devices," *Mechatronics*, 10(4–5): 555–569.
- Chapman EG, Herdic SL, Keller CA and Lynch CS (2005) "Development of Miniaturized Piezo-Hydraulic Pumps," In: *Proceedings of the SPIE*, Vol. 5762, SPIE, San Diego, CA, pp. 299–310. DOI:10.1117/12.605967.
- Chaudhuri A (2008) "Self-Contained Hybrid Electro-Hydraulic Actuators Using Magnetostrictive and Electrostrictive Materials," PhD Thesis, Department of Aerospace Engineering, University of Maryland, College Park, MD.
- Chaudhuri A and Wereley NM (2007) "Dynamic Model of a Hybrid Hydraulic Actuator Utilizing Different Smart Materials," In: *Proceedings of the ASME International Mechanical Engineering Congress and Exposition*, Paper no. IMECE2007-42557, pp. 193–202, ASME, Seattle, WA. DOI:10.1115/IMECE2007-42557.
- Chaudhuri A and Wereley NM (2008) "Design and Testing of a PMN-PT Based Compact Hybrid Actuator," In: *ASME Conference on Smart Materials, Adaptive Structures and Intelligent Systems*, Paper no. SMASIS2008-495, pp. 763–774, ASME, Ellicott City, MD. DOI:10.1115/SMASIS2008-495.
- Chaudhuri A and Wereley NM (2010) "Experimental Validation of a Hybrid Electrostrictive Hydraulic Actuator Analysis," *ASME Journal of Vibration and Acoustics*, 132(2), 021006 (11 pages). DOI:10.1115/1.4000778.
- Chaudhuri A, Yoo J-H and Wereley NM (2006) "Dynamic Modeling of a Magnetostrictive Hydraulic Pump," In: *Proceedings of the ASME International Mechanical Engineering Congress and Exposition*, Paper No. IMECE2006-

- 15320, ASME, Chicago, IL. 71:331–338. DOI:10.1115/IMECE2006-15320.
- Chaudhuri A, Yoo J-H and Wereley NM (2009) “Design, Test and Model of a Hybrid Magnetostrictive Hydraulic Actuator,” *Smart Materials and Structures*, 18(8): 085019(21 pages). DOI: 10.1088/0964-1726/18/8/085019.
- Chaudhuri A, Yoo J-H, Wereley NM and Nersessian N (2006) “Scaling-Up Issues with a Magnetostrictive Hydraulic Pump,” In: *Proceedings of the ASME International Mechanical Engineering Congress and Exposition*, Paper no. IMECE2006-15695, pp. 403–408, ASME, Chicago, IL. DOI:10.1115/IMECE2006-15695.
- Cheng G-M, Li P, Zeng P, Dong J-S and Sun F-F (2007) “Piezoelectric Pump Used in Bionic Underwater Propulsion Unit,” *Journal of Bionic Engineering*, 4(3): 159–164. DOI: 10.1016/S1672-6529(07)60028-6.
- Chopra I (2000) “Status of Application of Smart Structures Technology to Rotorcraft Systems,” *Journal of American Helicopter Society*, 45(4): 228–252.
- Claeyssen F and Lhermet N (2002) “Actuators Based on Giant Magnetostrictive Materials,” In: *8th International Conference on New Actuators*, Bremen, Germany Messe Bremen GMBH, pp. 148–153.
- Claeyssen F, Lhermet N, Le Letty R and Bouchilloux P (1997) “Actuators, Transducers and Motors Based on Giant Magnetostrictive Materials,” *Journal of Alloys and Compounds*, 258(1–2): 61–73. DOI :10.1016/S0925-8388(97)00070-4.
- Clark AE, Spano ML and Savage HT (1983) “Effect of Stress on the Magnetostriction and Magnetization of Rare Earth-Fe 1.95 Alloys,” *IEEE Transactions on Magnetics*, 19(5): 1964–1966. DOI : 10.1109/TMAG.1983.1062692.
- Crawley EF (1987) “Intelligent Structures for Aerospace—A Technology Overview and Assessment,” *AIAA Journal*, 32(8): 1689–1699. DOI: 10.2514/3.12161.
- Culp GW and Nuys V (1993) “Apparatus and Method for Piezoelectric Pump,” *US Patent* 5,192,197.
- Cunningham G, Kee RJ and Kenny RG (1999) “Reed Valve Modelling in a Computational Fluid Dynamics Simulation of the Two-Stroke Engine,” *Proceedings of the Institution of Mechanical Engineers—Part D—Journal of Automobile Engineering*, 213(1): 37–45. DOI: 10.1243/0954407991526658.
- Dapino MJ (2004) “On Magnetostrictive Materials and Their Use in Adaptive Structures,” *Structural Engineering and Mechanics*, 17(3–4): 303–329.
- Dapino MJ, Flatau AB and Calkins FT (2006) “Statistical Analysis of Terfenol-D Material Properties,” *Journal of Intelligent Material Systems and Structures*, 17(7): 587–599. DOI: 10.1177/1045389X06059500.
- Dapino MJ, Smith RC and Flatau AB (2000) “A Model for the ΔE Effect in Magnetostrictive Transducers,” In: *Proceedings of the SPIE*, Vol. 3985, SPIE, San Diego, CA, pp. 174–185. DOI:10.1117/12.388821.
- Dapino MJ, Smith RC, Faidley LE and Flatau AB (2000) “A Coupled Structural-Magnetic Strain and Stress Model for Magnetostrictive Transducers,” *Journal of Intelligent Material Systems and Structures*, 11(2): 135–152. DOI: 10.1106/MJ6A-FBP9-9M61-0E1F.
- Das D and Arakeri JH (2000) “Unsteady Laminar Duct Flow with a Given Volume Flow Rate Variation,” *Journal of Applied Physics*, 67(2): 274–281. DOI: 10.1115/1.1304843.
- de Wit CC, Olsson H, Astrom KJ and Lischinsky P (1995) “A New Model of Control of Systems with Friction,” *IEEE Transactions on Automatic Control*, 40(3): 419–425. DOI: 10.1109/9.704999.
- Doebelin EO (1980) *System Modeling and Response: Theoretical and Experimental Approaches*, John Wiley & Sons Inc., New York.
- Ellison J (2004) “Investigation of Active Materials as Driving Elements in a Hydraulic-Hybrid Actuator,” Master’s Thesis, University of Maryland, College Park, MD.
- Ellison JA, Sirohi J and Chopra I (2004) “Design and Testing of a Bidirectional Magnetostrictive-Hydraulic Hybrid Actuator,” In: *Proceedings of the SPIE*, Vol. 5390, SPIE, San Diego, CA, pp. 483–494. DOI:10.1117/12.539919.
- Engdahl G (ed.) (1999) *Handbook of Giant Magnetostrictive Materials*, Academic Press, San Diego, CA.
- Faidley LE, Lund BJ, Flatau AB and Calkins FT (1998) “Terfenol-D Elastomagnetic Properties under Varied Operating Conditions Using Hysteresis Loop Analysis,” In: *Proceedings of the SPIE*, Vol. 3329, SPIE, San Diego, CA, pp. 856–865. DOI:10.1117/12.316956.
- Galloni EE and Kohen M (1979) “Influence of the Mass of the Spring on its Static and Dynamic Effects,” *American Journal of Physics*, 47(12): 1076–1078. DOI: 10.1119/1.11978.
- Garcia E (2002) “Smart Structures and Actuators: Past, Present, and Future,” In: *Proceedings of the SPIE: Industrial and Commercial Applications of Smart Structures Technologies*, Vol. 4698, SPIE, San Diego, CA, pp. 1–12. DOI: 10.1117/12.475054.
- Gerver MJ, Goldie JH, Swenbeck JR, Shea R, Jones P, Ilmonen RT, Dozor DM, Armstrong S, Roderick R, Nimblett FE and Iovanni R (1998) “Magnetostrictive Water Pump,” In: *Proceedings of the SPIE*, Vol. 3329, SPIE, San Diego, CA, pp. 694–705. DOI: 10.1117/12.316943.
- Ghidaoui MS (2004) “On the Fundamental Equations of Water Hammer,” *Urban Water Journal*, 1(2): 71–83. DOI: 10.1080/15730620412331290001.
- Giurgiutiu V (2000) “Review of Smart-Materials Actuation Solutions for Aeroelastic and Vibration Control,” *Journal of Intelligent Material Systems and Structures*, 11(7): 525–544. DOI: 10.1106/HYTV-NC7R-BCMM-W3CH.
- Giurgiutiu V and Pomirleanu R (2001) “Modeling and Characterization of Piezoelectric and Magnetostrictive Induced Strain Actuators,” In: *Proceedings of the SPIE*, Vol. 4327, SPIE, San Diego, CA, pp. 610–619. DOI: 10.1117/12.436569.
- Giurgiutiu V and Rogers CA (1996) “Dynamic Power and Energy Capabilities of Commercially-Available Electro-Active Induced-Strain Actuators,” *Journal of Intelligent Material Systems and Structures*, 7(6): 656–667. DOI: 10.1177/1045389X9600700605.
- Giurgiutiu V and Rogers CA (1997) “Power and Energy Characteristics of Solid-State Induced-Strain Actuators for Static and Dynamic Application,” *Journal of Intelligent Material Systems and Structures*, 8(9): 738–750. DOI: 10.1177/1045389X9700800903.
- Giurgiutiu V, Chaudhry Z and Rogers CA (1995) “Engineering Feasibility of Induced Strain Actuators for Rotor Blade Active Vibration Control,” *Journal of Intelligent Material Systems and Structures*, 6(5): 583–597. DOI: 10.1243/09544070JAUTO1292.

- Giurgiutiu V, Rogers CA and Chaudhry Z (1996) "Energy-Based Comparison of Solid-State Induced-Strain Actuators," *Journal of Intelligent Material Systems and Structures*, 7(1): 4–14. DOI: 10.1177/1045389X9600700101.
- Giurgiutiu V, Rogers CA and Chaudhry Z (1997) "Design of Displacement-Amplified Induced-Strain Actuators for Maximum Energy Output," *Journal of Mechanical Design*, 119(4): 511–517. DOI: 10.1115/1.2826397.
- Hall DL and Flatau AB (1993) "Nonlinearities, Harmonics, and Trends in Dynamic Applications of Terfenol-D," In: *Proceedings of the SPIE*, Vol. 1917, SPIE, San Diego, CA, pp. 929–939. DOI: 10.1117/12.152822.
- Heverly DE II, Wang KW and Smith EC (2004) "Dual-Stack Piezoelectric Device with Bidirectional Actuation and Improved Performance," *Journal of Intelligent Material Systems and Structures*, 15(7): 565–574. DOI: 10.1177/1045389X04044450.
- Hom CL and Shankar N (1994) "A Fully Coupled Constitutive Model for Electrostrictive Ceramic Models," *Journal of Intelligent Material Systems and Structures*, 5(6): 795–801. DOI: 10.1177/1045389X9400500610.
- Hom CL and Shankar N (1997) "Modeling the Dynamic Behavior of Electrostrictive Actuators," In: *Proceedings of the SPIE*, Vol. 3041, SPIE, San Diego, CA, pp. 268–280. DOI: 10.1117/12.275652.
- Hom CL and Shankar N (1999) "Constitutive Model for Relaxor Ferroelectrics," In: *Proceedings of the SPIE*, Vol. 3667, SPIE, San Diego, CA, pp. 134–144. DOI: 10.1117/12.350068.
- Hurst WE (2002) "Piezohydraulic Actuator Design and Modeling Using a Lumped-Parameter Approach," Master's Thesis, Virginia Polytechnic Institute and State University, Blacksburg, VA.
- John S (2007) "Development of a Magnetorheological Fluid Based Hybrid Actuator," PhD Thesis, Department of Aerospace Engineering, University of Maryland, College Park, MD.
- John S, Cadou C, Yoo J-H and Wereley NM (2006) "Application of CFD in the Design and Analysis of a Piezoelectric Hydraulic Pump," *Journal of Intelligent Material Systems and Structures*, 17(11): 967–979. DOI: 10.1177/1045389X06062142.
- John S, Chaudhuri A and Wereley NM (2008) "A Magnetorheological Actuation System: Test and Model," *Smart Materials and Structures*, 17(2): 025023(15 pages). DOI: 10.1088/0964-1726/17/2/025023.
- John S, Chaudhuri A, Cadou C and Wereley NM (2009) "Unsteady Fluid Flow in Hybrid Hydraulic Actuators," *Journal of Intelligent Material Systems and Structures*, 20(18): 2201–2214. DOI: 10.1177/1045389X09348926.
- John S, Sirohi J, Wang G and Wereley NM (2006) "Comparison of Piezoelectric, Magnetostrictive and Electrostrictive Hybrid Hydraulic Actuators," In: *Proceedings of the ASME International Mechanical Engineering Congress and Exposition*, Paper no. IMECE2006-15698, ASME, Chicago, IL, pp. 409–418. doi:10.1115/IMECE2006-15698.
- John S, Sirohi J, Wang G and Wereley NM (2007) "Comparison of Piezoelectric, Magnetostrictive, and Electrostrictive Hybrid Hydraulic Actuators," *Journal of Intelligent Material Systems and Structures*, 18(10): 1035–1048. DOI: 10.1177/1045389X06072355.
- John S, Wereley NM and Sirohi J (2009) "Development of a Piezohydraulic Active Pitch Link for a Swashplateless Helicopter Rotor," *Journal of Aircraft*, 46(1): 328–331. DOI: 10.2514/1.36661.
- John S, Yoo JH and Wereley NM (2007) "A Magnetorheological Actuation System—Part I: Testing," In: *Proceedings of the ASME International Design Engineering Technical Conferences Paper no. DETC2007-35646*, ASME, Las Vegas, NV, pp. 239–248. DOI: 10.1115/DETC2007-35646.
- Junwu K, Zhigang Y, Taijiang P, Guangming C and Boda W (2005) "Design and Test of a High-Performance Piezoelectric Micropump for Drug Delivery," *Sensors and Actuators A: Physical*, 121(1): 156–161. DOI: 10.1016/j.sna.2004.12.002.
- Kan J, Tang K, Ren Y, Zhu G and Li P (2009) "Study on a Piezohydraulic Pump for Linear Actuators," *Sensors and Actuators A: Physical*, 149(2): 331–339. DOI: 10.1016/j.sna.2008.12.008.
- Karnopp D (1985) "Computer Simulation of Stick-Slip Friction in Mechanical Dynamic Systems," *Journal of Dynamic Systems, Measurement and Control*, 107(1): 100–103.
- Kellogg R and Flatau AB (2001) "Stress-Strain Relationship in Terfenol-D," In: *Proceedings of the SPIE*, Vol. 4327, SPIE, San Diego, CA, pp. 541–549. DOI: 10.1117/12.436583.
- Kellogg RA and Flatau AB (2004) "Blocked-Force Characteristics of Terfenol-D Transducers," *Journal of Intelligent Material Systems and Structures*, 15(2): 117–128. DOI: 10.1177/1045389X04039830.
- Keoschkerjan R, Harutyunyan M and Wurmus H (2002) "Analysis of Self-Heating Phenomenon of Piezoelectric Microcomponents Actuated Harmonically," *Microsystem Technologies*, 9(1–2): 75–80. DOI: 10.1007/s00542-002-0198-2.
- Kim GW and Wang KW (2007) "Piezoelectric-Hydraulic Pump Based Band Brake Actuation System for Automotive Transmission Control," In: *Proceedings of the SPIE*, Vol. 6525, SPIE, San Diego, CA, pp. 65251E1–65251E10, DOI: 10.1117/12.714929.
- Kim GW and Wang KW (2009) "Enhanced Control Performance of a Piezoelectric-Hydraulic Pump Actuator for Automotive Transmission Shift Control," *Proceedings of the Institution of Mechanical Engineers, Part D: Journal of Automobile Engineering*, 224(2): 161–174. DOI: 10.1243/09544070JAUTO1292.
- Kim GW and Wang KW (2009) "On-Line Estimation of Effective Bulk Modulus in Fluid Power Systems Using Piezoelectric Transducer Impedance," *Journal of Intelligent Material Systems and Structures*, 20(17): 2101–2106. DOI: 10.1177/1045389X09345558.
- Kim GW and Wang KW (2009) "Switching Sliding Mode Force Tracking Control of Piezoelectric-Hydraulic Pump-Based Friction Element Actuation Systems for Automotive Transmissions," *Smart Materials and Structures*, 18(8): 085004(15 pages). DOI: 10.1088/0964-1726/18/8/085004.
- Kinetic Ceramics Inc. "Piezoelectric Fluid Pumps," http://www.kineticceramics.com/piez_fluid.html. Accessed Sept. 5, 2011.
- Konishi K (1995) "Hydraulic Actuators Driven by Piezoelectric Elements," In: *Proceedings of the International Symposium on Microsystems, Intelligent Materials and Robots*, Sendai, Japan, pp. 362–365.

- Konishi K, Yoshimura T, Hashimoto K and Yamamoto N (1993) "Hydraulic Actuators Driven by Piezoelectric Elements (1st Report, Trial Piezoelectric Pump and Its Maximum Power)," *Transactions of the Japan Society of Mechanical Engineers C*, 59(564): 2477–2484.
- Lai T and Kay P (1993) "Breakaway Frictions of Dynamic O-Rings in Mechanical Seals," *Lubrication Engineering*, 49(5): 349–356.
- Lee DG, Or SW and Carman GP (2004) "Design of a Piezoelectric-Hydraulic Pump with Active Valves," *Journal of Intelligent Material Systems and Structures*, 15(2): 107–115. DOI: 10.1177/1045389X04039730.
- Lee DY and Wereley NM (1999) "Quasi-steady Herschel-Bulkley Analysis of Electro-and Magnetorheological Flow Mode Dampers," *Journal of Intelligent Material Systems and Structures*, 10(10): 761–769. DOI: 10.1106/E3LT-LYN6-KMT2-VJJD.
- Leo DJ (2007) *Engineering Analysis of Smart Material Systems*. John Wiley & Sons, Inc., Hoboken, NJ.
- Lhermet N, Delas O and Claeysen F (2006) "Magnetostrictive Pump with Piezo Active Valves for More Electrical Aircraft," In: *10th International Conference on New Actuators*, Bremen, Germany, Messe Bremen GMBH, pp. 964–967.
- Liang C, Sun FP and Rogers CA (1994) "Coupled Electromechanical Analysis of Adaptive Material System—Determination of the Actuator Power Consumption and System Energy Transfer," *Journal of Intelligent Material Systems and Structures*, 5(1): 12–20. DOI: 10.1177/1045389X9400500102.
- Liang C, Sun FP and Rogers CA (1996) "Electro-Mechanical Impedance Modeling of Active Material Systems," *Smart Materials and Structures*, 5(2): 171–186. DOI: 10.1088/0964-1726/5/2/006.
- Liang C, Sun FP and Rogers CA (1997) "An Impedance Method for Dynamic Analysis of Active Material Systems," *Journal of Intelligent Material Systems and Structures*, 8(4): 323–334. DOI: 10.1177/1045389X9700800405.
- Lindler JE, Anderson EH and Regelbrugge ME (2003) "Design and Testing of Piezoelectric-Hydraulic Actuators," In: *Proceedings of the SPIE*, Vol. 5054, SPIE, San Diego, CA, pp. 96–107. DOI: 10.1117/12.483888
- Loewy RG (1997) "Recent Developments in Smart Structures with Aeronautical Applications," *Smart Materials and Structures*, 6(5): R11–R42.
- Manring ND (2005) *Hydraulic Control Systems*, John Wiley & Sons Inc., New York.
- Mauck LD and Lynch CS (1999) "Piezoelectric Hydraulic Pump," In: *Proceedings of the SPIE*, Vol. 3668, SPIE, San Diego, CA, pp. 844–852. DOI: 10.1117/12.350760.
- Mauck LD and Lynch CS (2000) "Piezoelectric Hydraulic Pump Development," *Journal of Intelligent Material Systems and Structures*, 11(10): 758–764. DOI: 10.1106/HC2A-ABR9-21H8-2TJB.
- Mauck LD, Menchaca J and Lynch CS (2000) "Piezoelectric Hydraulic Pump Development," In: *Proceedings of the SPIE*, Vol. 3985, SPIE, San Diego, CA, pp. 729–739. DOI: 10.1117/12.388881.
- Merritt HE (1967) *Hydraulic Control Systems*, John Wiley & Sons Inc., New York.
- Mitrovic M, Carman GP and Straub FK (1999) "Electro-Mechanical Characterization of Piezoelectric Stack Actuators," In: *Proceedings of the SPIE*, Vol. 3668, SPIE, San Diego, CA, pp. 586–601, DOI:10.1117/12.350689.
- Moffett MB, Clark AE, Wun-Fogle M, Lindberg J, Teter JP and McLaughlin EA (1991) "Characterization of Terfenol-D for Magnetostrictive Transducers," *Journal of the Acoustical Society of America*, 89(3): 1448–1455. DOI: 10.1121/1.400678.
- Naik T, Longmire EK and Mantell SC (2002) "Dynamic Response of a Cantilever in Liquid near a Solid Wall," *Sensors and Actuators A: Physical*, 102(3): 240–254. DOI: 10.1016/S0924-4247(02)00398-9.
- Nasser K (2000) "Development and Analysis of the Lumped Parameter Model of a Piezohydraulic Actuator," Master's Thesis, Virginia Polytechnic Institute and State University, Blacksburg, VA.
- Nasser K and Leo DJ (2000) "Efficiency of Frequency-Rectified Piezohydraulic and Piezopneumatic Actuation," *Journal of Intelligent Material Systems and Structures*, 11(10): 798–814. DOI: 10.1106/KE26-P84N-78XD-DG34.
- Nasser K, Leo DJ and Cudney HH (2000) "Compact Piezohydraulic Actuation System," In: *Proceedings of the SPIE*, Vol. 3991, SPIE, San Diego, CA, pp. 312–322. DOI: 10.1117/12.388174.
- Nasser K, Vujic N, Leo DJ and Cudney HH (2001) "Modeling and Testing of a Piezohydraulic Actuation System," In: *Proceedings of the SPIE*, Vol. 4327, SPIE, San Diego, CA, pp. 354–365. DOI: 10.1117/12.436547.
- Nersessian N, Chaudhuri A, John S, Wang G and Wereley NM (2007) "Blocked Force and Free Displacement Characterization of PMN-32% PT Stacks," In: *Proceedings of the SPIE*, Vol. 6526, SPIE, San Diego, CA, 652603, DOI: 10.1117/12.716349.
- Niezrecki C, Brei D, Balakrishnan S and Moskalik A (2001) "Piezoelectric Actuation: State of the Art," *The Shock and Vibration Digest*, 33(4): 269–280.
- Niezrecki C, Schueller JK and Balasubramanian K (2004) "Piezoelectric-Based Fluid Bulk Modulus Sensor," *Journal of Intelligent Material Systems and Structures*, 15(12): 893–899. DOI: 10.1177/1045389X04045151.
- Nosse DT and Dapino MJ (2005) "Compact Actuation through Magnetorheological Flow Control and Rectification of Magnetostrictive Vibrations," In: *Proceedings of the SPIE*, Vol. 5764, SPIE, San Diego, CA, pp. 262–273. DOI:10.1117/12.605444.
- Nosse DT and Dapino MJ (2007) "Magnetorheological Valve for Hybrid Electrohydrostatic Actuation," *Journal of Intelligent Material Systems and Structures*, 18(11): 1121–1136. DOI: 10.1177/1045389X06072359.
- Oates WS and Lynch CS (2001) "Piezoelectric Hydraulic Pump System Dynamic Model," *Journal of Intelligent Material Systems and Structures*, 12(11): 737–744. DOI: 10.1177/104538901400438037.
- Ogawa K, Yoshida Y, Nishizawa M, Kamehara N, Yano A, Miyaki A, Ono M, Numata Y, Kurihara K and Watanabe K (1999) "Piezoelectric Pumps," *US Patent* 5,798,600.
- Olsson H, Astrom KJ, Canudas de Wit C, Gafvert M and Lischinsky P (1998) "Friction Models and Friction Compensation," *European Journal of Control*, 4(3): 176–195.
- Parker Hannifin Corporation. (2001) *Parker O-Ring Handbook*, Parker Hannifin Corporation, Cleveland, OH.
- Petitnot J-L, des Rochettes H.-M and Leconte P (2002) "Experimental Assessment and Further Development of

- Amplified Piezo Actuators for Active Flap Devices,” In: *8th International Conference on New Actuators*, Bremen, Germany, Messe Bremen GMBH.
- Phulé PP (2001) “Magnetorheological (MR) Fluids: Principles and Applications,” *Smart Materials Bulletin*, 2001(2): 7–10.
- Regelbrugge ME, Lindler J and Anderson EH (2003) “Design model for Piezohydraulic Actuators,” In: *44th AIAA/ASME/ASCE/AHS/ASC Structures, Structural Dynamics and Materials Conference, Paper No. AIAA-2003-1640*, AIAA, Norfolk, VA, pp. 2163–2171.
- Richer E and Hurmuzlu Y (2000) “A High Performance Pneumatic Force Actuator System: Part I—Nonlinear Mathematical Model,” *Journal of Dynamic Systems, Measurement, and Control—Transactions of the ASME*, 122(3): 416–425. DOI: 10.1115/1.1286336.
- Ronkanen P, Kallio P, Vilkkio M and Koivo HN (2004) “Self Heating of Piezoelectric Actuators: Measurement and Compensation,” In: *Proceedings of the 2004 IEEE International Symposium on Micro-Nanomechanics and Human Science, IEEE*, Piscataway, NJ, pp. 313–318.
- Rupinsky MJ and Dapino MJ (2006) “Smart Material Electrohydrostatic Actuator for Intelligent Transportation Systems,” In: *Proceedings of the ASME International Mechanical Engineering Congress and Exposition*, Paper no. IMECE2006-14542, ASME, Chicago, IL, pp. 721–730. DOI: 10.1115/IMECE2006-14542.
- Sager FE and Matice CJ (1998) “Piezoelectric Pumps,” *US Patent* 5,798,600.
- Santos FC, Coutinho YA, Ribeiro-Pinto L and Tort AC (2006) “The Motion of Two Masses Coupled to a Finite Mass Spring,” *European Journal of Physics*, 27(5): 1037–1051. DOI: 10.1088/0143-0807/27/5/003.
- Sirohi J (2002) Piezoelectric Hydraulic Hybrid Actuator for a Potential Smart Rotor Application, PhD Thesis, Department of Aerospace Engineering, University of Maryland, College Park, MD.
- Sirohi J and Chopra I (2003) “Design and Development of a High Pumping Frequency Piezoelectric-Hydraulic Hybrid Actuator,” *Journal of Intelligent Material Systems and Structures*, 14(3): 135–147. DOI: 10.1177/1045389X03014003002.
- Sirohi J and Chopra I (2001) “Development of a Compact Piezoelectric-Hydraulic Hybrid Actuator,” In: *Proceedings of the SPIE*, Vol. 4327, SPIE, San Diego, CA, pp. 401–412. DOI: 10.1117/12.436551.
- Sirohi J, Cadou C and Chopra I (2003) “Frequency Domain Modeling of a Piezohydraulic Actuator,” In: *44th AIAA/ASME/ASCE/AHS/ASC Structures, Structural Dynamics and Materials Conference, Paper No. AIAA-2003-1641*, AIAA, Norfolk, VA. (13 pages)
- Sirohi J, Cadou C and Chopra I (2005) “Investigation of the Dynamic Characteristics of a Piezohydraulic Actuator,” *Journal of Intelligent Material Systems and Structures*, 16(6): 481–492. DOI: 10.1177/1045389X05051072.
- Smith RC (1997) “Modeling Techniques for Magnetostrictive Actuators,” In: *Proceedings of the SPIE*, Vol. 3041, SPIE, San Diego, CA, pp. 243–253. DOI: 10.1117/12.275690.
- Sneed R, Smith RR, Cash MF and Anderson EH (2007) “Smart-Material Based Hydraulic Pump System for Actuation of a Morphing Wing,” In: *15th AIAA/ASME/AHS Adaptive Structures Conference, Paper No. AIAA-2007-1702*, AIAA, Honolulu, Hawaii, (10 pages).
- Sneed R, Smith RR, Cash MF, Bales GL and Anderson EH (2006) “Development of Smart Material—Hydraulic Pumps and Actuators,” In: *Proceedings of ASME International Mechanical Engineering Congress and Exposition, ASME*, Chicago, IL, IMECE2006-15896, pp. 435–443. DOI: 10.1115/IMECE2006-15896.
- Szymanski P (1932) “Some Exact Solutions of the Hydrodynamic Equations of a Viscous Fluid in the Case of a Cylindrical Tube,” *Journal of Pure and Applied Mathematics*, 11(9): 67.
- Tan H (2002) “Performance Modeling and Efficiency Analysis for a Piezoelectric Pump with Active Valves,” Master’s Thesis, Virginia Polytechnic Institute and State University, Blacksburg, VA.
- Tan H, Hurst W and Leo D (2005) “Performance Modeling of a Piezohydraulic Actuation System with Active Valves,” *Smart Materials and Structures*, 14(1): 91–110. DOI: 10.1088/0964-1726/14/1/010.
- Tang P, Palazzolo AB, Kascak AF and Montague G (1997) “Electromechanical Modeling of Hybrid Piezohydraulic Actuator System for Active Vibration Control,” *Journal of Dynamic Systems, Measurement and Control*, 119(1): 10–18. DOI: 10.1115/1.2801199.
- Tang P, Palazzolo AB, Kascak AF, Montague G and Li W (1995) “Combined Piezoelectric-Hydraulic Actuator Based Active Vibration Control for Rotordynamic System,” *ASME Journal of Vibration and Acoustics*, 117(3): 285–293. DOI: 10.1115/1.2874449.
- Tarnopolsky AZ, Lai JCS and Fletcher NH (2002) “Aerodynamic Damping of Randomly Excited Plates in Stationary and Moving Air,” *Journal of Sound and Vibration*, 253(4): 795–805. DOI: 10.1006/jsvi.2001.3805.
- The Lee Company (2006) *Technical Hydraulic Handbook*, the Lee Company, Westbrook, CN.
- Tieck RM, Carman GP, Lin Y and O’Neill C (2005) “Characterization of a Piezohydraulic Actuator,” In: *Proceedings of the SPIE*, Vol. 5764, SPIE, San Diego, CA, pp. 671–679, DOI: 10.1117/12.605351.
- Uchida S (1956) “The Pulsating Viscous Flow Superposed on the Steady Laminar Motion of Incompressible Fluids in a Circular Pipe,” *Zeitschrift für Angewandte Mathematik und Physik*, 7(5): 403–422.
- Ullmann A and Fono I (2002) “The Piezoelectric Valve-Less Pump—Improved Dynamic Model,” *Journal of Microelectromechanical Systems*, 11(6): 655–664. DOI: 10.1109/JMEMS.2002.805048.
- Ullmann A, Fono I and Taitel Y (2001) “The Piezoelectric Valve-Less Pump—Dynamic Model,” *Journal of Fluids Engineering—Transactions of the ASME*, 123(1): 92–98. DOI: 10.1115/1.1343459.
- Wallach DL, Beatty W, Beisler K, Chronowski P, Holloway M, Hutchinson R, Kacmarik D, Lesko R, Lutz J, Miller D and Sivak M (1988) “The Effect of the Mass of the Center Spring in One-Dimensional Coupled Harmonic Oscillators,” *American Journal of Physics*, 56(12): 1120–1123. DOI: 10.1119/1.15735.
- Walters TE (2008) “Development of a Smart Material Electrohydrostatic Actuator Considering Rectification Valve Dynamics and In Situ Valve Characterization,” Master’s Thesis, the Ohio State University, Columbus, OH.
- Wan Y, Fang D and Hwang KC (2003) “Non-Linear Constitutive Relations for Magnetostrictive Materials,”

- International Journal of Non-Linear Mechanics*, 38:1053–1065. DOI: 10.1016/S0020-7462(02)00052-5.
- Watton J (1989) *Fluid Power Systems: Modeling, Simulation, Analog and Microcomputer Control*, Prentice Hall, UK.
- Wereley NM and Pang L (1998) “Nondimensional Analysis of Semi-Active Electrorheological and Magnetorheological Dampers Using Approximate Parallel Plate Models,” *Smart Materials and Structures*, 7(5): 732–743. DOI: 10.1088/0964-1726/7/5/015.
- Wereley NM (2008) “Nondimensional Herschel-Bulkley Analysis of Magnetorheological and Electrorheological Dampers.” *Journal of Intelligent Material Systems and Structures*, 19(3): 257–268. DOI: 10.1177/1045389X07088107.
- White FM (1979) *Viscous Fluid Flow*, McGraw-Hill Book Company, New York.
- Wylie EB and Streeter VL (1983) *Fluid Transients*, FEB Press, Ann Arbor, MI.
- Yoo J-H and Wereley NM (2002) “Design of a High-Efficiency Magnetorheological Valve,” *Journal of Intelligent Material Systems and Structures*, 13(10): 679–685. DOI: 10.1177/1045389X02013010012
- Yoo J-H and Wereley NM (2004) “Performance of a Magnetorheological Hydraulic Power Actuation System,” *Journal of Intelligent Material Systems and Structures*, 15(11): 847–858. DOI: 10.1177/1045389X04044536.
- Yoo J-H and Wereley NM (2005) “Non-Dimensional Analysis of Annular Duct Flow in Magnetorheological/Electrorheological Dampers,” *International Journal of Modern Physics B*, 19(7–9): 1577–1583. DOI: 10.1142/S021797920503061X.
- Yoo J-H, Sirohi J and Wereley NM (2005) “A Magnetorheological Piezohydraulic Actuator,” *Journal of Intelligent Material Systems and Structures*, 16(11–12): 945–953. DOI: 10.1177/1045389X05053914.
- Yoo J-H, Sirohi J, Wereley NM and Chopra I (2003) “A Magnetorheological Hydraulic Actuator Driven by a Piezopump,” In: *Proceedings of the SPIE*, Vol. 5056, SPIE, San Diego, CA, pp. 444–456. DOI: 10.1117/12.483497.
- Yoo J-H, Sirohi J, Wereley NM and Chopra I (2004) “Bidirectional Control of a Magnetorheological Piezohydraulic Actuator,” In: *Proceedings of the SPIE*, Vol. 5390, SPIE, San Diego, CA, pp. 116–1261, DOI: 10.1117/12.547577.